



Roller Testing to Mimic Damage of the ISS SARJ Ring and Durability Test to Simulate 15 Years of SARJ Operation Using the Damaged Surface

*Timothy L. Krantz, Justin P. Elchert, Christopher DellaCorte, and Michael J. Dube
Glenn Research Center, Cleveland, Ohio*

NASA STI Program . . . in Profile

Since its founding, NASA has been dedicated to the advancement of aeronautics and space science. The NASA Scientific and Technical Information (STI) Program plays a key part in helping NASA maintain this important role.

The NASA STI Program operates under the auspices of the Agency Chief Information Officer. It collects, organizes, provides for archiving, and disseminates NASA's STI. The NASA STI Program provides access to the NASA Technical Report Server—Registered (NTRS Reg) and NASA Technical Report Server—Public (NTRS) thus providing one of the largest collections of aeronautical and space science STI in the world. Results are published in both non-NASA channels and by NASA in the NASA STI Report Series, which includes the following report types:

- **TECHNICAL PUBLICATION.** Reports of completed research or a major significant phase of research that present the results of NASA programs and include extensive data or theoretical analysis. Includes compilations of significant scientific and technical data and information deemed to be of continuing reference value. NASA counter-part of peer-reviewed formal professional papers, but has less stringent limitations on manuscript length and extent of graphic presentations.
- **TECHNICAL MEMORANDUM.** Scientific and technical findings that are preliminary or of specialized interest, e.g., “quick-release” reports, working papers, and bibliographies that contain minimal annotation. Does not contain extensive analysis.
- **CONTRACTOR REPORT.** Scientific and technical findings by NASA-sponsored contractors and grantees.
- **CONFERENCE PUBLICATION.** Collected papers from scientific and technical conferences, symposia, seminars, or other meetings sponsored or co-sponsored by NASA.
- **SPECIAL PUBLICATION.** Scientific, technical, or historical information from NASA programs, projects, and missions, often concerned with subjects having substantial public interest.
- **TECHNICAL TRANSLATION.** English-language translations of foreign scientific and technical material pertinent to NASA's mission.

For more information about the NASA STI program, see the following:

- Access the NASA STI program home page at <http://www.sti.nasa.gov>
- E-mail your question to help@sti.nasa.gov
- Fax your question to the NASA STI Information Desk at 757-864-6500
- Telephone the NASA STI Information Desk at 757-864-9658
- Write to:
NASA STI Program
Mail Stop 148
NASA Langley Research Center
Hampton, VA 23681-2199



Roller Testing to Mimic Damage of the ISS SARJ Ring and Durability Test to Simulate 15 Years of SARJ Operation Using the Damaged Surface

*Timothy L. Krantz, Justin P. Elchert, Christopher DellaCorte, and Michael J. Dube
Glenn Research Center, Cleveland, Ohio*

National Aeronautics and
Space Administration

Glenn Research Center
Cleveland, Ohio 44135

Acknowledgments

This work was supported by the NASA Engineering Safety Center (NESC). We thank Dr. Malcolm Stanford, NASA Glenn Research Center, for assistance with metallographic inspections and interpretations and Mr. Richard Manco, Sierra Lobo, Inc., for test operations support and documentation including profilometry and photography.

Level of Review: This material has been technically reviewed by technical management.

Available from

NASA STI Program
Mail Stop 148
NASA Langley Research Center
Hampton, VA 23681-2199

National Technical Information Service
5285 Port Royal Road
Springfield, VA 22161
703-605-6000

This report is available in electronic form at <http://www.sti.nasa.gov/> and <http://ntrs.nasa.gov/>

Roller Testing to Mimic Damage of the ISS SARJ Ring and Durability Test to Simulate 15 Years of SARJ Operation Using the Damaged Surface

Timothy L. Krantz, Justin P. Elchert, Christopher DellaCorte, and Michael J. Dube
National Aeronautics and Space Administration
Glenn Research Center
Cleveland, Ohio 44135

Abstract

The International Space Station's starboard Solar Alpha Rotary Joint (SARJ) experienced a breakdown of the joint's race ring surface. The starboard SARJ mechanism was cleaned and lubricated with grease. To provide some guidance on the expected behavior of the damaged SARJ ring with continued operations, experiments were conducted using rollers and a vacuum roller test rig. The approach of the experimental work involved three main steps: (1) initiate damage using conditions representative of the SARJ with inadequate lubrication; (2) propagate the damage by operating the test rollers without lubrication; and (3) assess the durability of the roller by testing to simulate the equivalent of 15 years of SARJ operation on the damaged surface assuming adequate grease lubrication. During the rig testing, additional and/or replacement grease was introduced at regular intervals to maintain good lubrication in the rig. The damage to the nitride layer continued even after application of grease. The grease lubrication proved to be effective for limiting the value of the axial force that can be developed. Limiting the axial force on the SARJ mechanism is important since the larger the axial force the more concentrated the load pressure becomes on the blend-radius location on the SARJ roller. After the testing simulating 15 years of SARJ operations, the wear depths were the order of 0.2 mm for the nitrided 15-5 roller and the order of 0.06 mm for the mating 440C roller. Metallographic inspections were done to search for indications of impending fatigue or other fracture indications that might eventually propagate and cause structural failure. There were no indications or features found that could eventually compromise structural integrity.

Introduction

The International Space Station (ISS) makes use of a roller-based mechanism for positioning of the solar arrays. The fundamental concept of the roller-based mechanism of the ISS Solar Alpha Rotary Joint (SARJ) is described by Loewenthal and Schuller (Ref. 1). The starboard SARJ was launched in 2007 and began operation late in the year. After 16 days of operation, the drive torque and vibration began to rise. In late 2007 and early 2008, Extra Vehicular Activities (EVA) were conducted to inspect the starboard mechanism to determine the reasons for its poor performance. During the first such EVA, metallic wear debris was detected. Further inspections following continued use of the SARJ showed widespread wear debris and damage to one of the primary contact surfaces. A photograph of the damage to the SARJ ring is provided in Figure 1. The roughened surface shown in the figure is the mating surface for a set of rollers. The damaged surface is 15-5 steel that was provided with a nitrided treatment. The nitrided layer was applied with intended depth of about 0.15 mm (0.007 in.). Some of the debris has been returned to earth and analyzed. The debris has been determined to be primarily nitrided 15-5 PH steel (Ref. 2). The breakup of the race ring has been at least partially attributed to inadequate lubrication of the race ring and the contacting rollers (Ref. 2). Late in 2008 the starboard SARJ mechanism was cleaned and lubricated with grease.



Figure 1.—Damaged surface of a SARJ ring.

There exist several options to manage the continued operation of the SARJ mechanism. For example, a configuration change could allow for operation of the SARJ while avoiding the use of the damaged race ring as a mating surface for the rotating roller members. However, continued operation of the SARJ without such a configuration change is an attractive option. It is of practical interest to assess the long-term durability and structural integrity of the starboard SARJ mechanism operating with rollers interacting with the damaged ring race surface. The experience of the railroad industry to assess the integrity of railway rails perhaps provides some related theoretical guidance (Refs. 3 and 4). However, the theoretical guidance is not mature enough to allow for confident assessment of expected behavior directly by analysis. To provide some guidance on the expected behavior of the damaged SARJ ring with continued operations, experiments were conducted using rollers and a roller test rig. The approach of the experimental work involved three main steps: (1) initiate damage using conditions representative of the SARJ with inadequate lubrication; (2) propagate the damage by operating the test rollers without lubrication; and (3) assess the durability of the roller by testing to simulate the equivalent of 15 years of SARJ operation on the damaged surface assuming adequate grease lubrication.

Experimental Apparatus, Specimens, and Procedures

Test Apparatus for Roller Pairs

Testing was done using the NASA Glenn Research Center's Vacuum Roller Rig (Fig. 2). The rig allows for application and measurement of a load pressing the rollers together while having a purposely misaligned and adjustable shaft angle. The rig is depicted in schematic form in Figure 3. A drive motor provides motion to the driving roller. A magnetic-particle brake attached to the output shaft imposes torque on the driven roller. The rig can be operated with the brake not energized. For such a condition the torque transmitted through the roller pair is only the drag torque of the output shaft (drag of the seals and support bearings). The normal load pressing the rollers together is provided by an air cylinder. The cylinder acts through a gimbal point to rotate the plate that mounts the driving shaft and drive motor. The rotation of the drive motor plate displaces the driving roller toward the driven roller shaft. The pressure to the cylinder, and thereby the load between the contacting rollers, is adjusted by a hand-operated valve (open-loop control). Testing can be done in vacuum or ambient air. Vacuum is provided by a diffusion pump with a liquid nitrogen cold trap. The diffusion pump is assisted by a mechanical vacuum pump. Figure 4 provides a simplified schematic labeled with some of the nomenclature used herein.

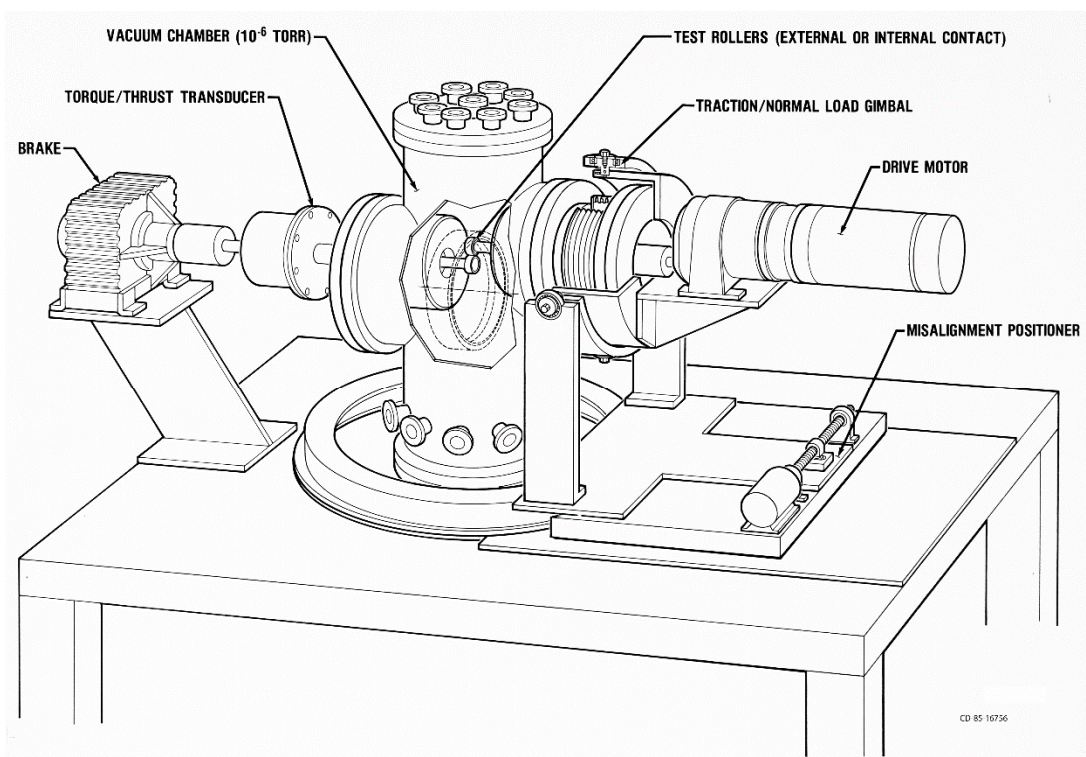


Figure 2.—Vacuum roller rig.

A set of sensors on the test apparatus monitors the test conditions. The outputs of the analog sensors were digitized and stored at a rate of 0.66 Hertz. Each of the sensors and the methods of calibration will be described in turn.

The misalignment of the driving roller shaft and driven roller shaft is depicted in an exaggerated manner in Figure 3(b). The misalignment is measured via a linear variable differential transformer (LVDT). The transducer housing is attached to the bedplate, and the translating, spring-loaded transducer tip contacts against a mechanical stop on the turntable. The mechanical stop is mounted at a known radial distance and tangential orientation from the center of the turntable. Calibrated gage blocks were used to displace the transducer by known amounts, and using the rig geometry the equivalent angular rotation of the turntable was calculated. The preceding steps established the relationship of change in transducer output to the change in relative shaft angle. To establish the aligned condition, a special tooling block was machined to locate the roller-mounting surfaces of the two shafts as parallel. With the shafts aligned by the tooling block, the transducer circuit balance was adjusted to provide an output of zero. The precision of this method for aligning the shafts was limited by the dimensions of the roller mounting surfaces used as the reference planes. From the test rig drawing tolerances and geometry, the alignment procedure using the tooling block to define the zero-degree position has an absolute accuracy of no better than 0.11° .

The torque on the output shaft is monitored by a strain-gage type torquemeter of 22 N-m (200 in.-lb) torque capacity. Calibration was done in place using deadweights acting on a torque arm of known length.

The load that presses the rollers together is termed herein the “normal load” (Fig. 4). The normal load is applied via an air-pressure actuated piston. The air piston acts through a load cell against the drive motor plate that is gimbal-mounted relative to the test chamber (Fig. 3(a)). In this way the air cylinder moves the roller on the input shaft in an arc motion toward the test roller. Once the rollers are in contact, additional force commanded from the air cylinder increases the normal load between the test rollers. The force sensed by the load cell located between the gimballed motor plate and the air piston is a linear combination of two sources, the unbalanced mass relative to the gimbal point and the normal load on the test roller.

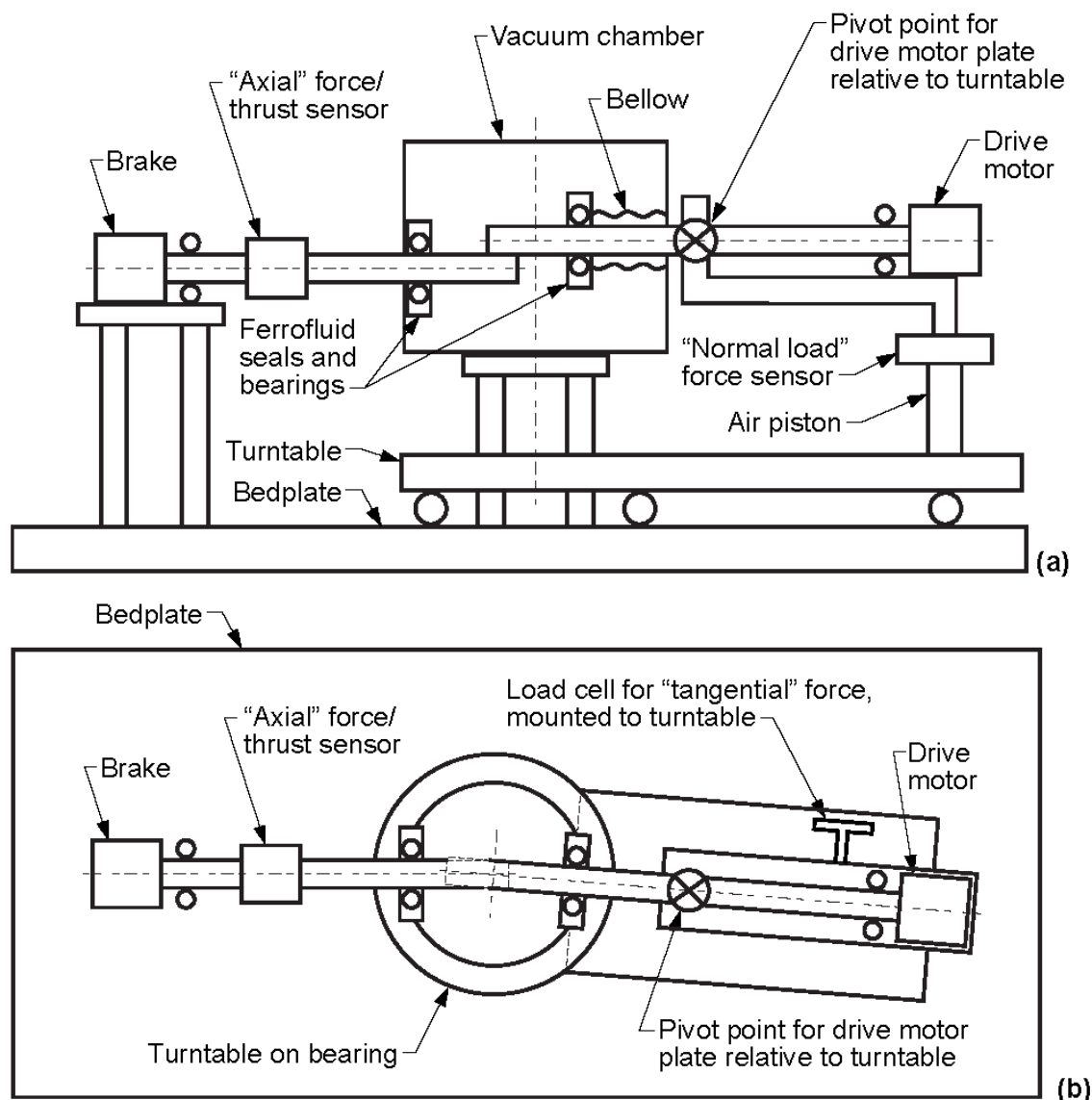


Figure 3.—Schematic views of the vacuum roller rig. (a) Schematic, side view. (b) Schematic, overhead view with shaft misalignment depicted and exaggerated.

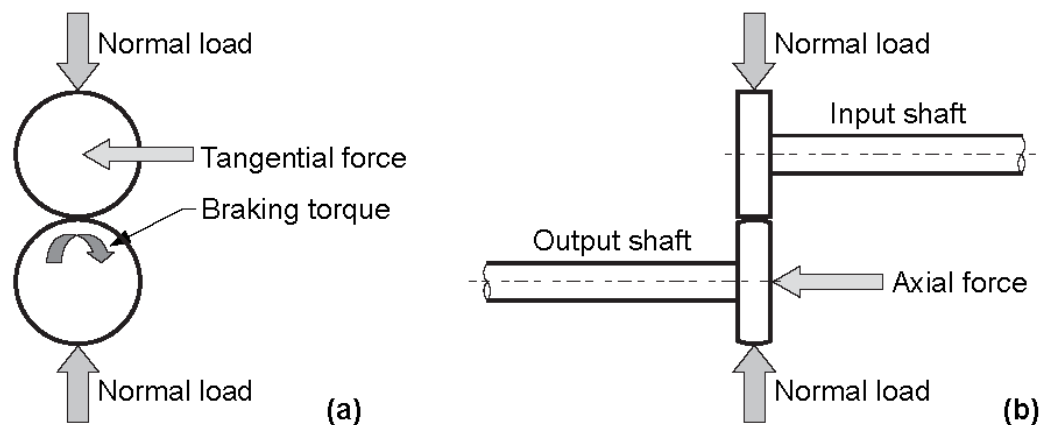


Figure 4.—Simplified schematic view including some of the important sensed data. (a) Schematic, front view. (b) Schematic, side view.

The following calibration procedure was used so that the two sources influencing the load cell output during testing could be separated. First the load cell was removed from the rig, calibrated using deadweights, and reinstalled on the test apparatus. Next, an LVDT was used to monitor the displacement of the motor plate. With no test roller installed on the output shaft, the air piston was used to move the motor plate through the full range of motion while recording the output of the calibrated load cell. In this manner the force as sensed at the load cell due to the unbalanced mass of the gimbaled motor plate was determined as a function of the motor plate position. Next, the end of the input shaft where the test roller is mounted was attached by a highly-rigid link to the apparatus frame. The rigid link included a calibrated reference load cell in the load path. The rigid link was carefully positioned to be oriented in the position and direction of the normal load created between the contacting test rollers. By increasing the pressure on the air-piston actuator, load was created on the rigid link and measured on the reference load cell. This procedure established the relationship of the normal load on the test roller acting through the gimbal point and resulting in a force imparted on the load cell located at the air piston. During testing both the motor table position and load cell force was recorded. From the table position data and calibration data, the force attributed to the unbalanced mass on the gimbaled motor plate could be subtracted from the force value recorded by the load cell. The value remaining from the load cell (after the subtraction operation) is due to the normal force between the test rollers, and via the calibration curve the load on the test roller is determined.

When rollers operate in a misaligned condition a force will develop in the direction of the shaft axis. In such a condition points on the two rollers in intimate contact and within a “stick” zone of the contact patch are constrained to move in unison. If the points were not in contact the kinematic constraints would provide a slightly different path of motion. The difference in the actual path of motion and that defined by the motion if the points were not in contact gives rise to surface strains and a resultant axial force. A sensor to measure this force is labeled as the “axial force” sensor in Figure 3. The axial force sensor is co-located on the output shaft with the torquemeter sensor. The configuration of the rig did not allow for direct deadweight calibration in place. To calibrate the sensor in place, the following procedure was used. First, a load cell was calibrated via deadweights and then was placed on the free end of the output shaft to act as a reference load cell. A threaded jackscrew acted against the reference load cell and a hard stop in the vacuum chamber. Adjusting the jackscrew length allowed for changing the force imparted on both the reference load cell and the rig’s axial load cell and to the machine frame. In this manner the same force was applied to both load cells, and the reference cell output used to calibrate the axial load cell sensor in place.

The preceding two paragraphs describe the sensors (and sensor calibrations) to determine two mutually perpendicular forces acting on the driven test roller. A force also acts along a third axis. This is the force directed tangential to the roller diameter and is termed here as the “tangential” force. The tangential force on the input shaft roller acts through a gimbal point (Fig. 3(b)). The rotational motion about the gimbal point is restrained by a mechanical link to the turntable structure. There is a load cell load in the load path from said mechanical link to the turntable structure. This sensor was calibrated in place by using a pulley-cable system and dead weights to relate the tangential force applied at the test roller position to the sensor output. During testing, this sensor is also affected by spin moments that can develop in roller contacts. The data from the tangential force sensor was recorded for possible future use, but such data were not of immediate interest and are not reported herein.

Shaft speeds and total number of shaft revolutions were measured using encoders on each shaft. The encoder pulses were counted and recorded via a digital pulse counter. The encoder pulses were also monitored by a frequency converter to provide a convenient shaft speed display to the test operator. The encoders provide 6,000 pulses for each shaft revolution.

The pressure in the chamber was monitored by an ionization gauge at the top of the main test chamber. The typical pressure in the testing chamber during vacuum testing was 5×10^{-6} torr. Vacuum is provided by a diffusion pump with a liquid nitrogen cold trap. The diffusion pump is assisted by a mechanical vacuum pump. The diffusion pump and cold trap arrangement prevents oil vapors from the mechanical vacuum pump to enter the test chamber so as to maintain the desired tribological test condition.

Test Specimens

The test rollers used for this research had a nominal geometry of 35.6 mm (1.40 in.) outer diameter and a 12.7 mm (0.50 in.) width. The roller on the drive motor (input) shaft was made from 15-5 steel alloy, matching the SARJ ring material. The 15-5 roller was nitrided following the manufacturing processes of the SARJ ring to produce a nitride layer of thickness of approximately 0.15 mm (0.007 in.). The core 15-5 roller material had a measured hardness via a Rockwell tester of 34 HRC. Three rollers were used for the brake (output) shaft, one roller for each of the three stages of testing comprising damage initiation, damage propagation, and durability assessment. The output shaft rollers were made from 440C steel alloy, matching the SARJ roller material. The 440C rollers had a measured surface hardness via a Rockwell tester of 55-57 HRC.

The manufactured geometries of the test rollers were inspected using a profilometer with a 2 μm radius conisphere tip stylus. To provide a controlled contact condition on the test apparatus, at least one of the two rollers must be crowned across the roller width. The 15-5 roller profile was designed as nominally flat, and the measured profile was found to be slightly concave (Fig. 5). The deviation in form from a flat profile was approximately 10 μm . The measured roughness of the nitrided roller in the direction of rolling is provided in Figure 6. Rollers made from 440C to mate with the nitride roller had differing form profiles for the initiation and propagation/durability phases of the testing. The SARJ rollers have a nominally flat profile with 45° angled chamfered ends with a blend radius transition from the flat region to the chamfered region. The 440C test roller used for damage initiation had geometry to mimic the blend radius used on the SARJ rollers. A cross-section view and measured roller profile for the specialized “blend-radius” roller are provided in Figure 7. The radius at the top of the roller per measurement was 1.5 mm. The 440C rollers used for damage propagation and durability testing had circular-crowned profiles across the roller of about 81 μm . The measured crown profile is provided in Figure 8. The roughness in the direction of rolling of the 440C roller used for durability testing is provided in Figure 9. Note the scaling of the ordinates when comparing to the roughness of the nitrided roller of Figure 6.

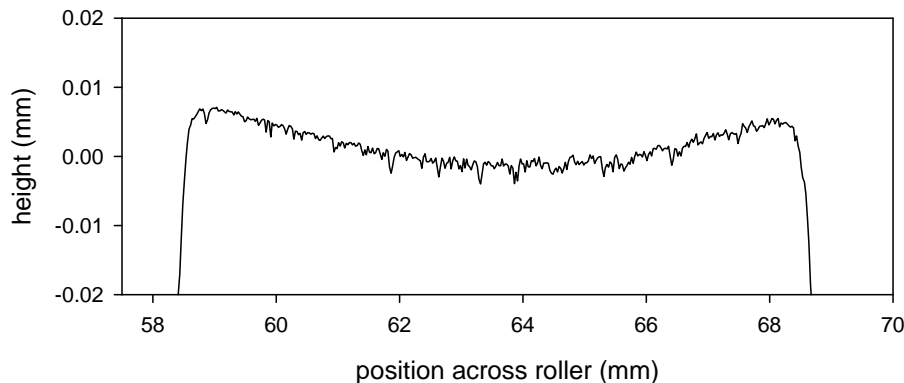


Figure 5.—Measured form of the nitrided 15-5 test roller in the direction of the roller width.

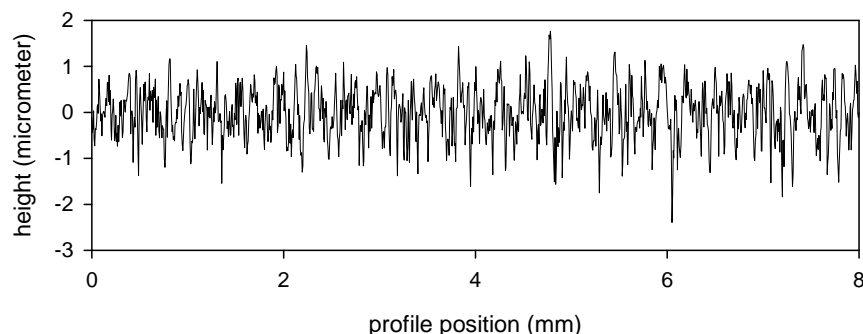


Figure 6.—Roughness of nitrided roller in the direction of rolling.

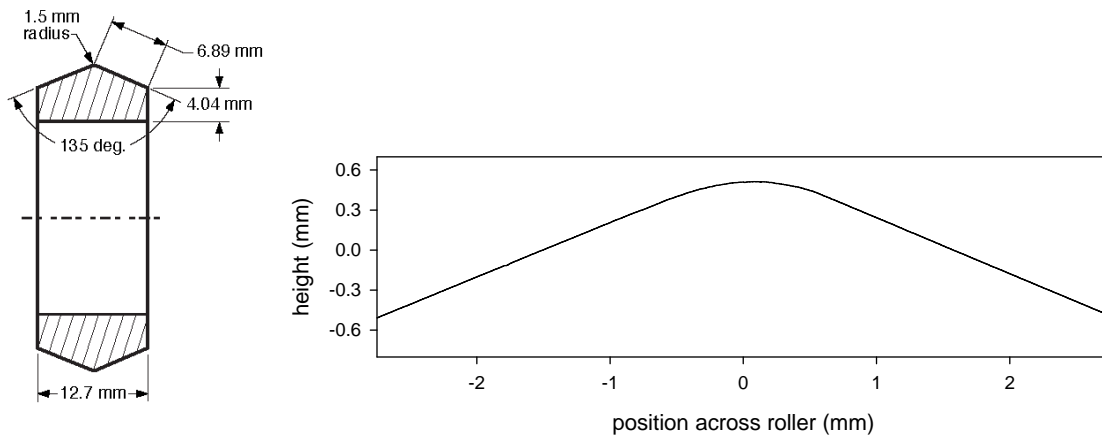


Figure 7.—Cross section view of roller design and the measured shape of the crown radius of the 440C “blend-radius” roller used for damage initiation.

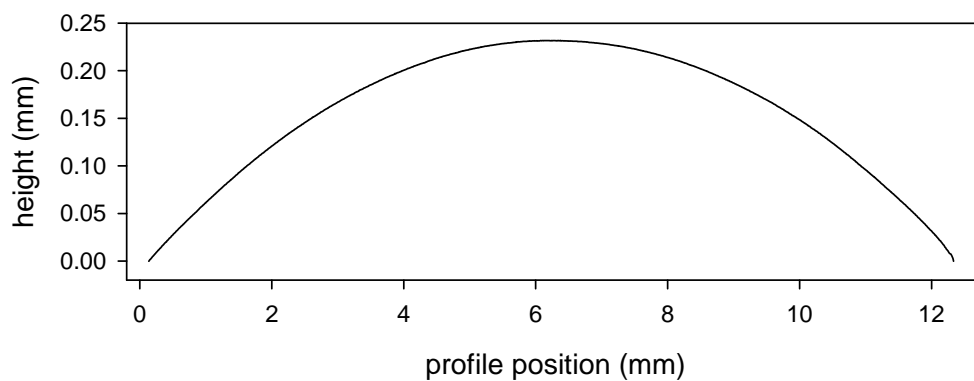


Figure 8.—Cross-section profile of 440C roller used for damage propagation and durability testing having crown radius of approximately 81 mm.

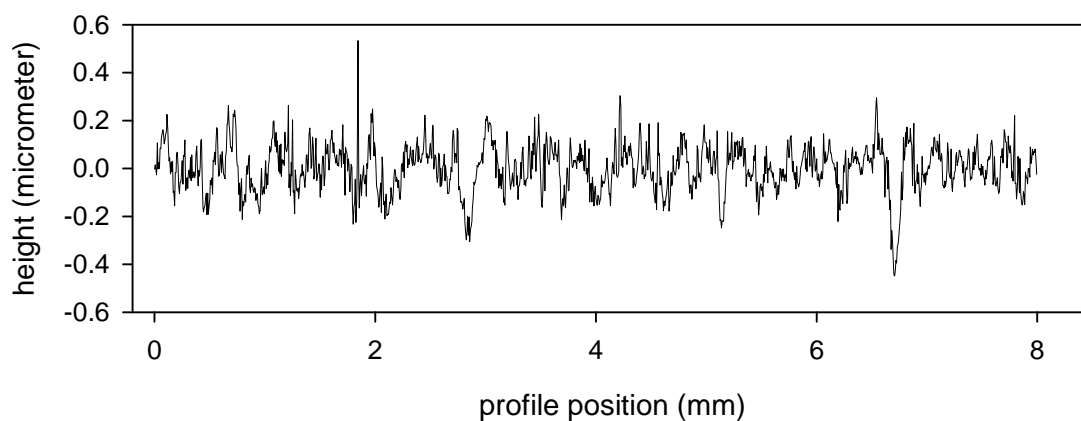


Figure 9.—Roughness of 440C roller used for damage propagation and durability testing.

Procedures for Cleaning, Installing, and Greasing Test Rollers

Test specimens were cleaned and installed using careful procedures to provide a clean test surface. The test rollers were cleaned just prior to installation into the rig using de-ionized water and 0.05 μm alumina powder. After appropriate hand scrubbing, the cleaning powder was rinsed with de-ionized water making sure that the entire roller surface wetted uniformly to confirm complete cleaning of surface oils. The rinsing water was removed from the rollers using dried pressurized nitrogen. Spacers used as an interface between the rig shafts and roller ends were likewise cleaned of surface oils. Test rollers and mounting hardware were handled only with gloved hands and clean tools to complete installation into the test apparatus.

After installation of the test rollers the testing chamber was immediately isolated and provided a vacuum, using the mechanical roughing pump, of approximately 50×10^{-3} torr chamber pressure. Just prior to testing the diffusion pump was energized and the pressure in the testing chamber established to approximately 5×10^{-6} torr.

For the durability phase of testing, rollers were lubricated using a space-qualified grease. The base oil of the grease is a stable perfluorinated polyether. The gelling agent is a tetrafluoroethylene telomer. The grease contains molybdenum disulfide. The grease was applied using a syringe. The difference in the mass of the syringe before and after applying the grease was recorded and was typically about 0.2 grams. The grease was distributed on the rollers by positioning the rollers with only a small gap between them and the shafts were rotated. As the grease became distributed by the shaft rotation the gap between the rollers was slowly reduced in increments. This action proved effective to distribute the grease about the roller circumference, and by visual inspection the distribution of the grease about the roller circumference appeared uniform (Fig. 10). As needed, the rollers were removed from the test apparatus for detailed inspection. In such cases, the grease was removed from the rollers using soft cloths for the inspections, and then grease was re-applied for the next increment of durability testing.

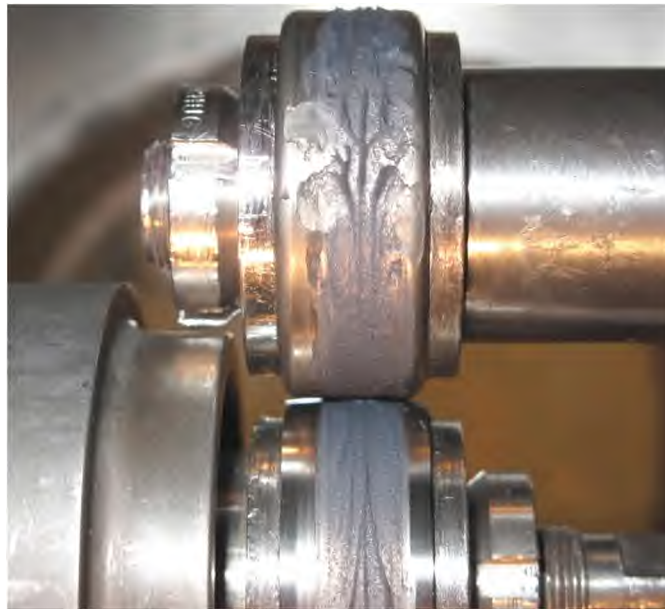


Figure 10.—Test rollers with grease applied and distributed to prepare for durability testing.

Roller Test Conditions and Relationships to SARJ Operating Conditions

The primary objective of this work was to study the durability of a damaged 15-5 nitrided surface that had been damaged and then subsequently operated in a well-lubricated condition. Engineering judgments were used to select test roller conditions to use the Vacuum Roller Rig so that the roller test results could be related to the SARJ mechanism and its operating conditions. Of course, the test apparatus imposed constraints on possible test scenarios. Test conditions (roller geometry, speed, normal load, and shaft angle) were selected considering several constraints. Some of the reasoning behind the engineering judgments and analysis results that guided those judgments will be described below for each of the three phases of testing (damage initiation, damage propagation, and durability assessment).

Test Conditions to Initiate Damage

To understand the loading conditions on SARJ mechanism rollers one needs to consider the influence of forces arising from misalignment of the rollers relative to the SARJ ring. Figure 11 illustrates the meaning of shaft misalignment. Kalker conducted pioneering research on the forces and moments that can arise from rollers in a variety of contact conditions (Ref. 5). The ground vehicle community has studied this phenomena for engineering of tires (Ref. 6). The SARJ rollers are constrained to rotate about shaft axes that nominally intersect the rotational axis of the ring (Fig. 11(a) and (b)). Any deviation from perfect alignment of a roller axis and ring axis (Fig. 11(c)) will give rise to a force at the contact interface in the direction of the roller shaft axis (termed herein the axial force). The magnitude of the axial force will depend on the magnitude of misalignment, the normal load on the roller, the stiffness of the system, the torque transmitted by the roller, and frictional condition of the contacting surfaces. The SARJ mechanism was built to high precision, and the installed roller shaft angle (misalignment) was within a fraction of a degree to perfect alignment. Still, misalignments of even such small magnitude can produce significant forces that influence the performance of the mechanism.

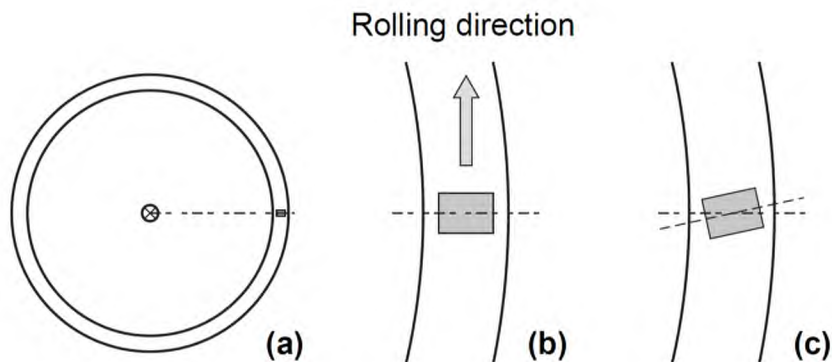


Figure 11.—SARJ ring and roller schematic, top view. (a) Overall view, roller axis aligned with ring axis; (b) overhead, close-up view near roller, aligned axis; (c) close-up view near roller, roller axis misaligned (misalignment magnitude greatly exaggerated).

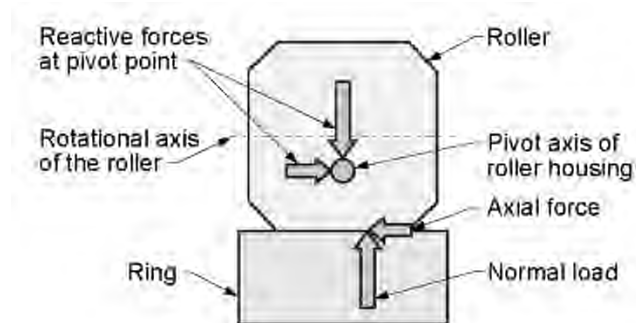


Figure 12.—Schematic of the SARJ roller and ring in contact, front view in cross-section.

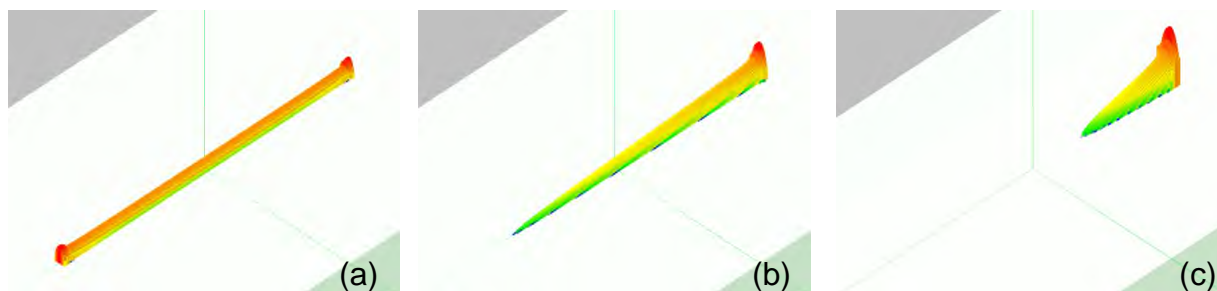


Figure 13.—Results of contact analysis of SARJ roller having the same normal load and three differing levels of axial load. (a) zero axial load, (b) axial load 0.18 times the normal load, (c) axial load 0.30 times the normal load.

For the condition of the roller shaft axis misaligned relative to the ring, a force will develop in the contact region directed coincident with the roller axis. This force is termed herein the “axial force”. The axial force is carried by a pair of tapered roller bearings via the roller shaft to the roller housing. The connection of the roller shaft to the housing is via a pivot point in the housing (Fig. 12). In the absence of misalignment, the pivot point allows for uniform contact pressures for the nominally flat roller profile contacting the nominally flat raceway surface. But for the case of misaligned axes, the axial force acts via the pivot point and produces a non-uniform contact pressure across the roller profile. Note from Figure 12 the moments created by the normal load and axial force acting via the pivot point must be balanced for static equilibrium. Thereby, the axial force acts to shift the position of the resultant normal load along the face of the ring and roller contact. The axial force arising from misaligned axes can cause tipping of the roller.

A contact analysis computer program based on the method discussed by Vijayakar (Ref. 7) was used to study the influence of the misaligned axis on the resultant roller-ring contact pressure. This analysis was done assuming that the pivot point in the roller housing provided negligible resistance to the overturning moment (some small resistance might be possible depending on the friction condition at the pivot point). Analysis results depicting contact pressures for three different values of overturning moment, as would result from three levels of axial force axial, are provided in Figure 13. Figure 13(a) shows the contact pressure produced by the roller on the ring for the idealized case of zero axial load as would happen for perfect alignment of the roller shaft and/or frictionless surfaces. The contact pressure is even across the width of the flat portion of the roller except for some pressure concentration at the location of the blend radius transitioning to the chamfer geometry. Figure 13(b) shows the contact pressure for the case of an axial load 0.18 times the normal load, as would occur for well-lubricated surfaces. Contact pressure is relieved from the left edge and concentrated at the blend-radius location toward the right edge. The shifting of the contact pressure is not too dramatic. Figure 13(c) shows the contact pressure for the case of axial load 0.30 times the normal load, as might represent marginal

lubrication (but not dry) condition. In this case, the contact pressure is concentrated over less than 1/3 of the available roller length, and the pressure carried in the region of the blend-radius is significant. In this case, the rigid body rotation of the roller was calculated to be about 0.2° of rotation, denoting a very slight tipping of the roller about the housing pivot point. Note that in the three plots of Figure 13, the contact pressures are scaled the same in each plot and so the plots can be compared to assess the relative pressure magnitudes. As is evident from these analyses results, the larger the axial force the larger is the fraction of the total contact pressure imposed on the blend radius region of the SARJ roller.

The Vacuum Roller Rig (VRR) used for this laboratory experiment does not include the degree-of-freedom provided by the pivot point in the SARJ mechanism housing. While in the SARJ mechanism the overturning moment created by the axial force is balanced by the shifting of the contact pressure (per Fig. 13), in the VRR the overturning moment is reacted directly by the shaft support bearings. To be able to simulate the effect of the contact pressure carried by the small blend radius of the SARJ roller, a special “blend-radius roller” was created for the VRR. The concept for the roller geometry is depicted in Figure 14. By employing this special roller, the VRR could be used to simulate the condition of a slightly tipped SARJ roller even though the tipping degree of freedom is not present in the VRR. A photo of the blend radius roller in the VRR is provided in Figure 15.

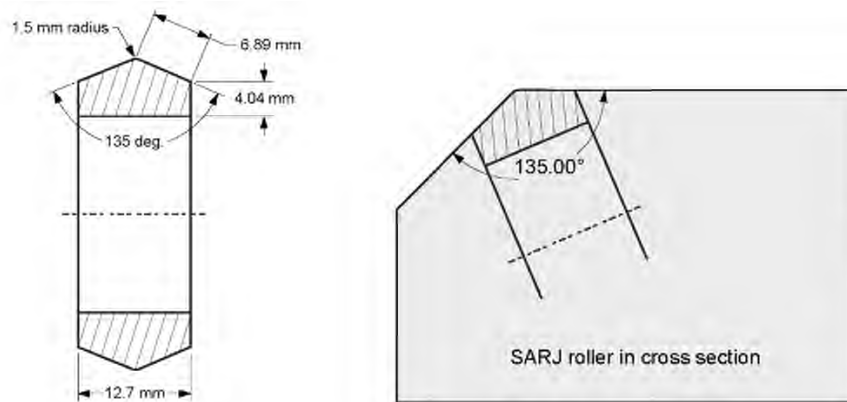


Figure 14.—Cross section of the “blend radius” roller and overlay of the roller shape on the SARJ roller cross section in the chamfer radius region.



Figure 15.—Photograph of the 440C blend radius roller on the lower shaft engaging a nitrided 15-5 roller on the upper shaft, simulating contact pressure concentration of chamfer blend radius on a SARJ roller.

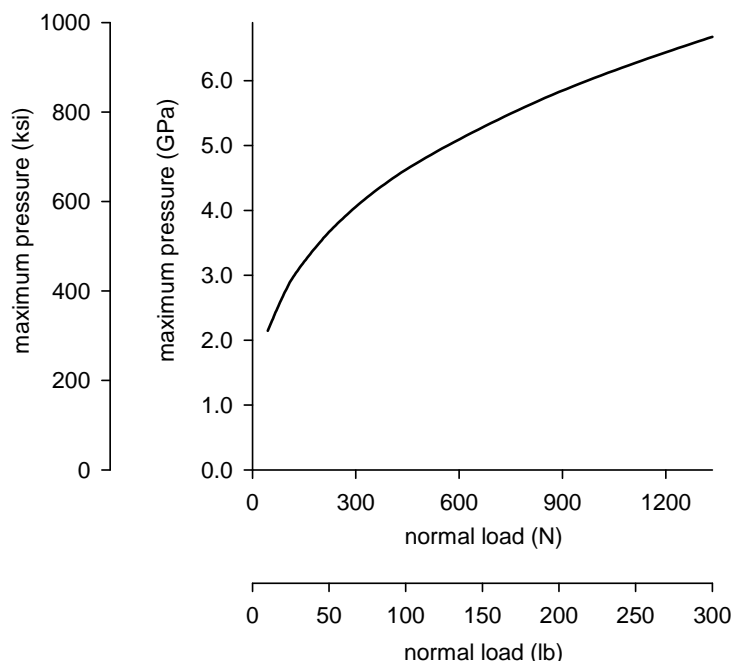


Figure 16.—Maximum Hertzian contact pressures obtained using the blend radius roller of Figures 14 and 15 for a range of normal loads assuming elastic response.

Having chosen the test roller geometry to mimic a tipped roller condition on the SARJ, the remaining test conditions to be chosen were the speed, shaft angle, and load. A speed of approximately 40 rpm was selected to satisfy practical considerations of operating time, speed of the data acquisition system, and desire to capture the test progress using digital video. The maximum shaft misalignment angle range of $\pm 1.5^\circ$ was used to maximize the axial force acting as a surface traction on the blend radius. To select loads, a Hertz contact analysis was completed. The maximum Hertzian (smooth surface) contact pressure as a function of load for the full rig normal load capability is provided in Figure 16. A starting load of about 300 N was selected expecting that such load would not produce damage initiation. After operation on the order of 500 to 1000 roller revolutions at a given load, the load was increased by about 200~250 N increments searching for a load condition that would initiate damage.

Test Conditions to Propagate Damage

The damage initiation testing provided damage to a relatively small region across the width of the roller. The damaged SARJ ring had damage across the majority of the available contact region of the ring surface. One can envision the SARJ rollers to contact the ring with varying amounts of tipping depending on the actual shaft alignment. Therefore, once damage was initiated on the SARJ ring, the edge of the damaged region could be engaged by a concentrated contact pressure via a roller tipped in a manner different from the one that initiated damage. To propagate the damage across the roller width in the test rig, the blend radius roller was removed and replaced by a roller having profile of a crown radius of about 81 mm. The profile of the damaged roller was measured, and the measurement data was used to define the roller geometry for contact analysis calculations. The calculated maximum contact pressure at positions across the roller width for a normal load of 910 N is provided in Figure 17. Also shown for comparison on the figure is the contact pressure if the roller were undamaged. We note that the damaged portion of the roller is essentially “bridged” by the crown-radius roller used for the damage propagation testing. Note that the contact pressures are about 1/2 order of magnitude greater for the damaged roller as compared to the undamaged roller and of similar magnitude as was produced by the blend-radius roller

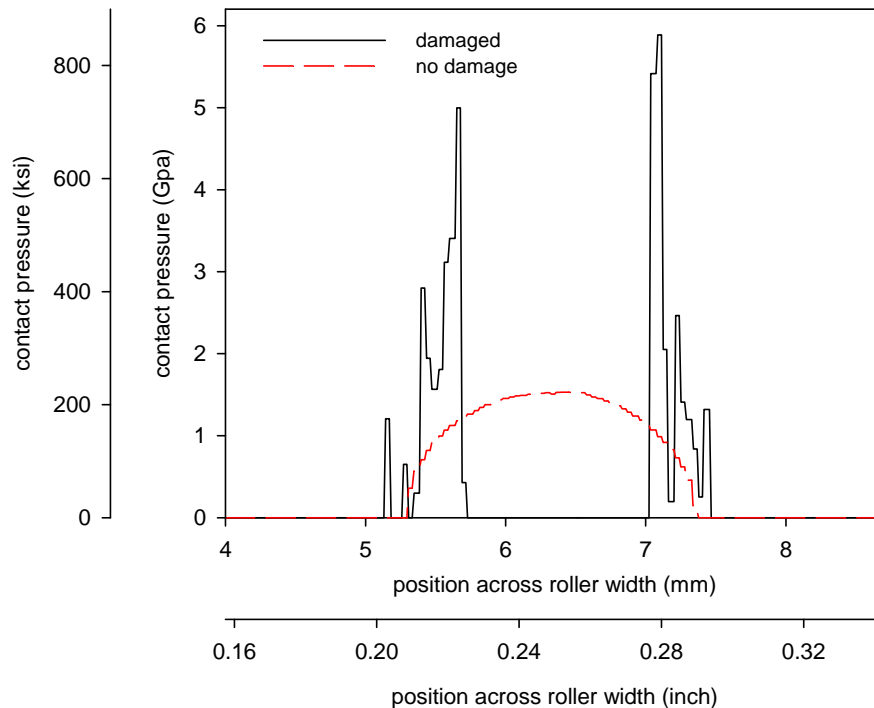


Figure 17.—Analytical prediction of maximum contact pressures at positions across the roller width after damage was initiated and then brought into contact with a new 81 mm crown-radius roller. The analyzed condition is a 910 N normal load. Also shown for comparison is the contact pressure for an undamaged roller.

used for damage initiation (Fig. 16). The test conditions for the damage propagation testing included no lubrication, a shaft misalignment angle of -0.7° , speed of 18 rev/min., and a normal load of about 900 N. These conditions were selected primarily by practical testing considerations. The testing duration to achieve damage propagation was a real-time judgment based on the visual appearance of the 15-5 roller surface as the damage progressed with the intent to replicate as close as possible the level of damage on the SARJ ring per EVA photographs.

Test Conditions to Study Roller Durability

After damage was initiated and propagated on the 15-5 roller, the roller was then mated with a new 440C roller having a crowned profile. The rollers were well-lubricated with grease during the durability testing. Test conditions for the durability testing needed to be selected. The primary mechanisms for degradation during the long term durability tests were not known beforehand with certainty. However, the likely potential degradation mechanisms were considered to be accelerated abrasive wear, adhesive wear, and spalling propagation of the 15-5 core material. Considering these mechanisms, test conditions were selected as follows.

Shaft Speed

First we will discuss the selection of the shaft speed. The testing was conducted in vacuum and with grease lubrication. The lubrication behavior provided by grease can, in general, be strongly influenced by the entraining velocity of the two surfaces in contact. A practical test constraint imposed by the test rig motor controller is a minimum testing speed of about 5 rev/min for the 5 rev/min test rig speed, the total entraining velocity of the two rollers is 0.73 in./sec. The total entraining velocity of the SARJ race and roller contact is 0.15 in./sec. Even at the slowest possible rig speed, the total entraining velocity pulling

lubricating oil into the contact was about five times greater in the test rig as compared to the SARJ mechanism. We considered that given the roughness of the damaged surfaces and slow speeds of the SARJ and the VRR, the lubrication provided would be primarily boundary lubrication. Therefore, the differences of entraining velocity were judged as a second order effect. Another aspect of selecting a testing speed was the practical consideration to accumulate the needed number of shaft revolutions in a reasonable testing time. At testing speeds of 100 rev/min, the rough roller surface produced a dynamic interaction with the loading piston and produced undesirable fluctuations of normal load. Testing at 80 rev/min did not produce these normal load fluctuations. Some testing was done at the slowest possible speed of 5 rev/min, and trends for the traction force were observed. The trends of traction forces as a function of shaft revolutions were similar at the 5 rev/min and the 80 rev/min testing speeds. Given all of these considerations, a testing speed of 80 rev/min was selected and used for the majority of the durability test.

Test Roller Normal Loads

Next we will discuss the selection of the test load applied to press the test rollers together (denoted as the normal load in Fig. 4). Keeping in mind the primary goal of the test was to assess the durability of the SARJ ring, the testing load was selected to mimic the contact pressure on the SARJ ring when a given region of the rotating ring passes under a roller. The contact region of the test rig and the SARJ mechanism differ because of the differing geometries and kinematic constraints. For the test rig the contact region is an ellipse shape while for the SARJ mechanism the contact region has an elongated triangular shape. Each roller on the SARJ mechanism can provide a slightly different contact pressure distribution depending on the normal load on the roller, the misalignment angle, and the lubrication condition of the ring-roller contact. The VRR test rig in its existing configuration does not allow for automated adjustment of load, and so a constant-load test was needed devised. We selected to mimic the contact pressure of a SARJ roller having a 4.5 kN (1000 lb) normal load and an axial load of 0.80 kN (180 lb). The axial load produces a net moment because of the camber degree of freedom in the roller housing, and so the pressure distribution features a shifting of the pressure toward the roller edge to create the balancing moment. The axial load/normal load ratio of 0.18 is a realistic value assuming good lubrication and a realistic value of roller misalignment of 0.35° . A contact analysis was completed for this loading of the SARJ roller-raceway in contact using software based on methods of Vijayakar (Ref. 7). The resulting pressure distribution as a contour map is provided in Figure 18. The maximum and mean pressures for the distribution of Figure 18 are 1600 MPa (230,000 psi) maximum and 470 MPa

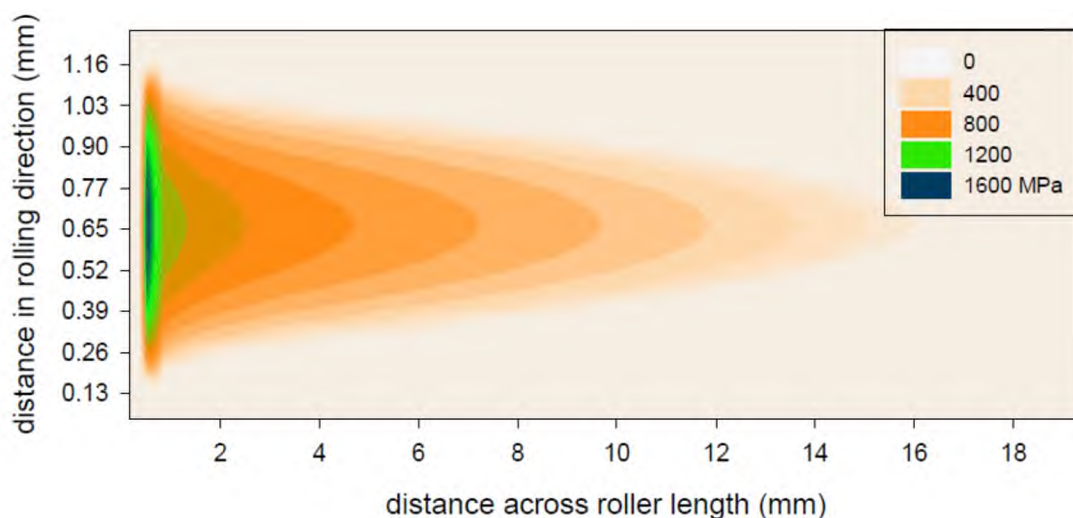


Figure 18.—Contour plot of calculated pressure distribution for SARJ roller and raceway operating with a 4500 N normal load and 800 N axial load.

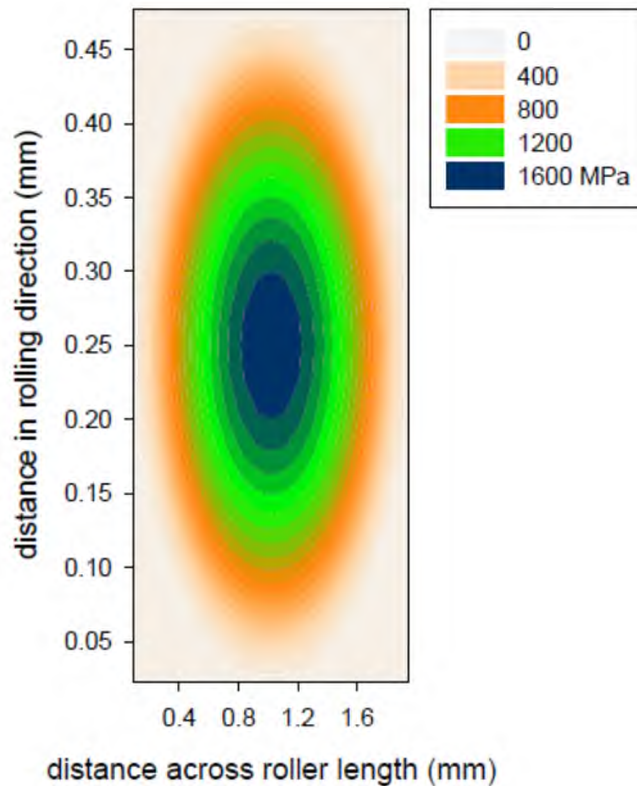


Figure 19.—Contour plot of calculated pressure distribution for vacuum roller rig operating with a 780 N normal load.

(68,000 psi) pressure mean values. The VRR test rig load was selected to approximate the pressure distribution of Figure 18, but because the test rig does not have the camber degree of freedom the mean and maximum pressures could not be matched simultaneously. So, a compromise approach was employed. After some iterative analysis, a testing load of 780 N (175 lb) was selected. A Hertzian contact analysis for this load was completed, and the calculated pressure distribution is provided in Figure 19. Note that for both Figures 18 and 19, the length of the ordinate is ten times greater than would provide a true aspect ratio plot. The distorted views were provided so that the distribution details could be depicted. The maximum and mean pressures for the distribution of Figure 19 are 1600 MPa (230,000 psi) maximum and 1000 MPa (154,000 psi) mean pressure values. We judged that this approach would provide some degree of conservatism for the purposes of assessing the material durability.

Misalignment Angle

Next we will discuss the selection of the misalignment angle of the test rollers. The misalignment is depicted in exaggerated manner in Figure 3. Deviation from perfect alignment of the roller axes causes the development of surface tractions (Ref. 5). The surface tractions occur since points in direct contact can be held together by contact friction and, thereby, deviate from the motion that would be occur if the roller was unconstrained by its mate. The deviation from free, unconstrained motion creates strains in the materials in contact. The contact region features both “stick and “slip” regions (Ref. 5). The magnitudes of the traction forces depend on the lubrication (friction) condition that thereby defines the transition from a stick to slip region. To a first order approximation, an approach to relate the SARJ misalignment angle and the test rig misalignment angle is to match the product of the contact region in the direction of rolling times the misalignment angle for both systems. Such an approach will provide for similar regions of sticking and slipping in terms of absolute distance. From Figures 18 and 19, we see that the maximum

size of the contact in the rolling direction in the region of high pressure is about two times greater for the SARJ roller as compared to the test rig roller. Therefore, the test rig misalignment angle was selected to be two times the angle of the SARJ misalignment to be mimicked. A subsequent independent contact analysis solving for the roller kinematics later confirmed that this first order approach using a shaft misalignment angle factor of two times provided a good matching of the axial loads that would develop (Ref. 8). The actual installed misalignment angles of a set of SARJ rollers have been completed (Ref. 9). Given all of the above data, a test rig misalignment angle of -0.7° was selected to mimic a -0.35° misalignment angle for the SARJ rollers. The -0.35° misalignment angle was selected as a representative condition, intending to represent an averaging effect of the set of 16 rollers that are in contact with a SARJ ring surface.

Test Duration

Next we will discuss the required test duration. The concept and goal of the test is to assess the durability of the damaged 15-5 steel race surface to survive 15 years of operation of the SARJ mechanism after damage of the nitrided surface. Each of the ring raceway surfaces are contacted by 16 rollers. Twelve of the rollers, from the trundle bearing assemblies, carry a relatively heavy load. Four of the rollers, from the drive lock assemblies, carry a relatively light load. We considered that even though the drive lock assembly rollers carry a relatively light load, the roller load can be concentrated over a relatively small region of the raceway depending on the misalignment angle of the roller axis and the lubrication condition. To devise a conservative test, we assumed that the rollers of the drive lock assembly could cause damage (wear, spall propagation, and/or fatigue) at the same rate as a trundle bearing assembly roller. A small region of the race ring surface therefore experiences 16 contact stress cycles for each revolution of the SARJ ring. The total number of stress cycles for 15 years of operation was calculated as:

$$\text{cycles} = (16 \text{ rollers/revolution}) \times (15.7 \text{ revolutions/day}) \times (365 \text{ days/year}) \times 15 \text{ years} = 1,375,000 \text{ cycles.}$$

Thereby, a test duration target of at least 1,375,000 revolutions of the 15-5 test roller was selected. We note that for the SARJ mechanism, the 440C rollers that mate with the 15-5 ring will experience more than this targeted number of stress cycles. The 15 year equivalency in terms of stress cycles selected herein applies only to the focus of this investigation, namely the damaged 15-5 ring. The testing was done assuming adequate grease lubrication throughout the 15 year operation. During the rig testing, grease lubrication was reapplied several times. The introduction of additional or new grease was done for any of the following reasons; (1) a persistent increase of the measured axial load above the magnitude for good lubrication, or (2) by visual assessment of a significant volume of wear debris particles, or (3) for practical scheduling of test monitoring and activities. Engineering judgment was used to balance the competing needs for re-greasing to maintain the best possible lubrication situation and the need for completion of the durability test in a time-efficient manner.

Experimental Results

The experimental results will be described for each of the three phases of the experiment: (a) damage initiation, (b) damage propagation, and (c) durability assessment. The results were documented via photographs, profilometer inspections, roller mass measurements, and after test completion destructive sectioning of the test roller for metallurgical assessments. Results for each of the three phases of the experiment are now described in turn.

Results of Damage Initiation Testing

The testing to initiate damage of the nitrided 15-5 test roller was done using a step-loading approach. After the first few load steps, some very minor damage and wear debris was noted. The test was interrupted at that time to open the test chamber for a close view of the rollers and to collect the wear debris for possible further analysis. Then the test chamber was closed, proper vacuum established, and the testing continued. During the second testing interval the load was again increased in steps, and a sudden and dramatic breakdown of the 15-5 roller surface occurred. The test continued for a short period of time after the damage initiation occurred to observe how quickly additional damage might accumulate, but additional operation after damage initiation was minimized to preserve the characteristics of the initiated damage. The conditions of the test roller surfaces during the test were monitored and recorded using a digital video camera.

Table 1 provides a summary of the test conditions used for the damage initiation testing. Testing was done at the maximum misalignment angle to provide large axial forces. The applied normal load was increased in steps starting at 302 N and increasing to 1134 N. The total duration of the test was 3544 shaft revolutions. The maximum Hertz contact pressures noted in Table 1 were calculated assuming elastic response. We recognize that the actual response of the rollers to the load will include plastic deformation for such large pressures, but the calculated values assuming elastic response provides a valuable measure of the load intensity. After the first three loading steps comprising a total of 2500 shaft revolutions (stress cycles), the test was interrupted so that the chamber could be opened and the wear debris could be collected. The wear debris had the appearance of fine, dry powder. After collection of the wear debris the chamber was closed, vacuum was established, and the testing continued so that more load could be induced.

During load step #5 of Table 1, more debris was generated including some needle-shaped debris that stood on end from the 440C roller surface. In Figure 20, a frame from the digital video recording, although somewhat out of focus because of the frame rate, shows the appearance of debris during load step #5. Similar debris of significant volume has been documented in photos of a trundle bearing assembly used on the damaged SARJ mechanism (Fig. 21).

TABLE 1.—TEST CONDITIONS FOR THE DAMAGE INITIATION TESTING

Step	Load (N)	Max. Hertz Pressure (GPa)	Speed (rpm)	Misalignment (degrees)	Cycles
1	302	4.1	42	1.5	520
2	503	4.8	42	1.5	720
3	712	5.4	42	1.5 then to -1.5	1260
chamber was opened to collect wear debris					
4	578	5.0	22	1.5	110
5	867	5.8	40	1.5 to -1.5	680
chipping event occurs during transition to next load					
6	1134	6.3	40	-1.5	88
7	1134	6.3	8	-1.5	166
Total cycles					3544

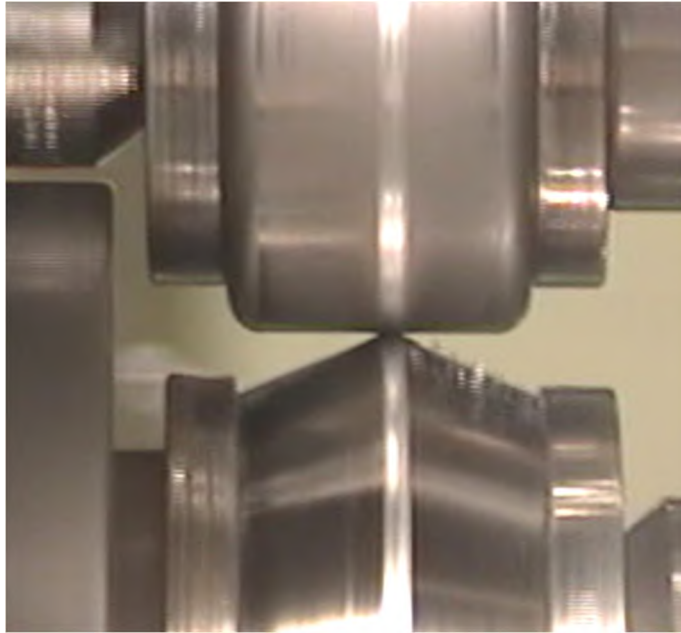


Figure 20.—Needle-shaped debris on the right side of the 440C roller (lower roller) as recorded during load step #5 of the damage initiation testing.



Figure 21.—Copious debris, including some needle-shaped debris, on a trundle bearing assembly that was mated with the damaged SARJ ring and returned from orbit for inspections.

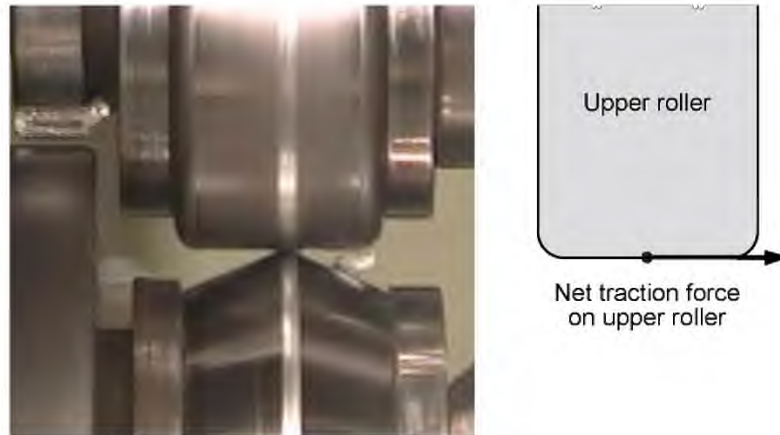


Figure 22.—Chip generating event captured on digital video. The chip is being liberated from the upper roller. The schematic shows the location and direction of the net axial force from traction on the upper roller.

During the transition from load step #5 to load step #6, a dramatic failure of the surface of the nitrided (upper) roller occurred and a large chip was liberated. Figure 22 is an image from the video recording showing the chip about to be liberated from the surface. The location of the chipped region included the zone adjacent to but outside of the immediate contact region reaching to the edge of the roller. Soon after the chipping event was noted, the rig speed was reduced so that the video could capture images of the chipped surface and additional damage propagation. After 245 shaft revolutions subsequent to the chipping event the test was stopped. Figure 22 has been augmented with a schematic showing the direction of the traction force imposed on the upper roller by the lower roller. Note that such a traction force will cause the nitrided layer to be in compression in the region where the chip was liberated. The measured axially directed traction force ranged from 434 to 512 N during the transition from load step #5 to load step #6 when the chipping failure occurred.

The visual appearance of the damage at the end of initiation testing is documented in Figures 23 and 24. Figure 23 shows the region where the large chip was liberated. Additional chipping outside of the narrow contact region is evident on both sides of the wear track. Figure 24 shows the region approximately one-half of a rotation around the circumference from the previous figure. Damage has occurred both within and adjacent to the wear track. The after-test condition of the mating 440C roller with the blend-radius geometry is provided in Figure 25. From this macroscopic view, it appears that there has been little change to this roller except for some minor wear and plastic deformation of asperity features.

To inspect the depth of the roller damage, a set of stylus profilometer inspections were completed. For the nitrided roller, inspections were made at eight circumferential locations of approximately equal spacing around the periphery. The mating 440C roller had the same appearance about the periphery, and so in this case only three equally spaced circumferential positions were selected for inspection. Results from selected positions will be discussed as follows. The inspection data at the location where the initial chip was liberated (location #7) is provided in Figure 26. The depth of the damage is to approximately tequal to the thickness of the nitrided layer. The inspection data of Figure 27 illustrates the typical damage away from the region of the initial large chip. At this location the depth of the damage is about one-half of the thickness of the nitrided layer. Some plastic flow of material rising above the location of the original surface (new condition) is evident at the edges of the wear track for both locations.

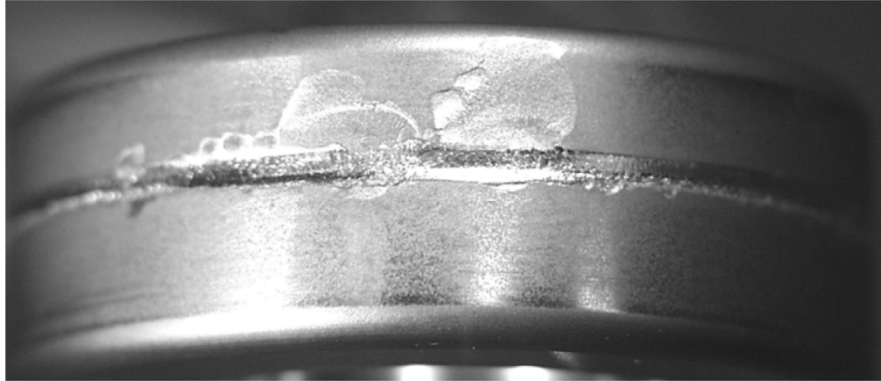


Figure 23.—Condition of the nitrided roller at the end of the damage initiation test. The circumferential location is the region where the large chip of Figure 22 was liberated.



Figure 24.—Condition of the nitrided roller at the end of the damage initiation test. The circumferential location is approximately 180° from the region of Figure 23.



Figure 25.—Condition of the 440C "blend-radius" geometry roller at the end of the damage-initiation test.

The condition of the mating 440C roller with blend-radius geometry at the tip was inspected after the test via the stylus profilometer. The data are presented in Figure 28 using true aspect ratio scaling to show the geometry shape and again in Figure 29 using an expanded ordinate to show details of the condition. From this data it appears that no significant debris was generated from the 440C roller, but significant gross plastic deformation did occur. The axially-directed traction force on the 440C roller was directed toward the right (positive x-direction) relative to the orientation used for inspections of Figures 26 and 27.

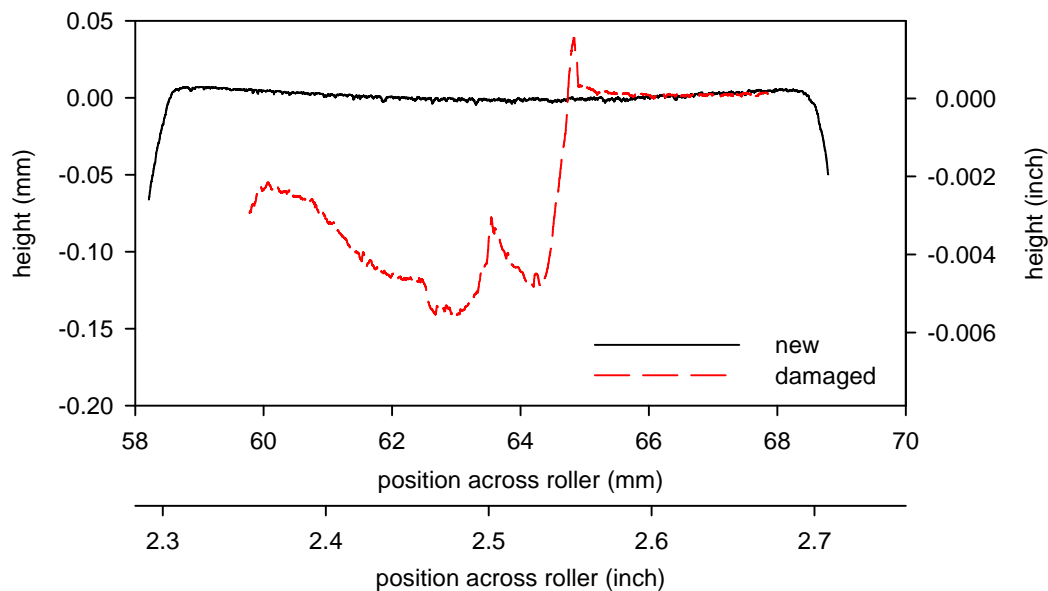


Figure 26.—Profilometer inspections of nitrided 15-5 roller at end of the damage initiation testing, circumferential position #7.

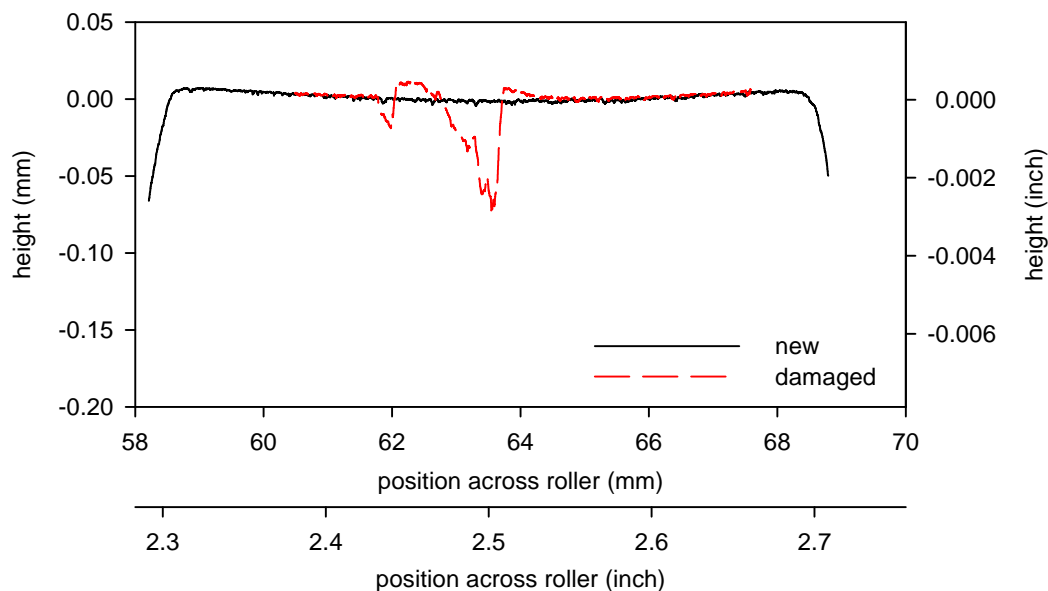


Figure 27.—Profilometer inspections of nitrided 15-5 roller at end of the damage initiation testing, circumferential position #5.

The roller masses were documented at the beginning and end of the damage-initiation testing. One can also estimate the mass change from profilometer data. Approximating the density of the nitrided 15-5 material as equal to that of steel and using the profilometer data of Figures 26 and 27, the mass change of the nitrided roller was estimated as a loss of 0.050 grams. The measured mass change of the nitrided 15-5 roller was 0.066 grams loss of mass. The profile data of Figure 28 suggests that the 440C roller mass increased during testing. The measured change of the 440C roller was 0.18 grams mass increase at the end of testing.

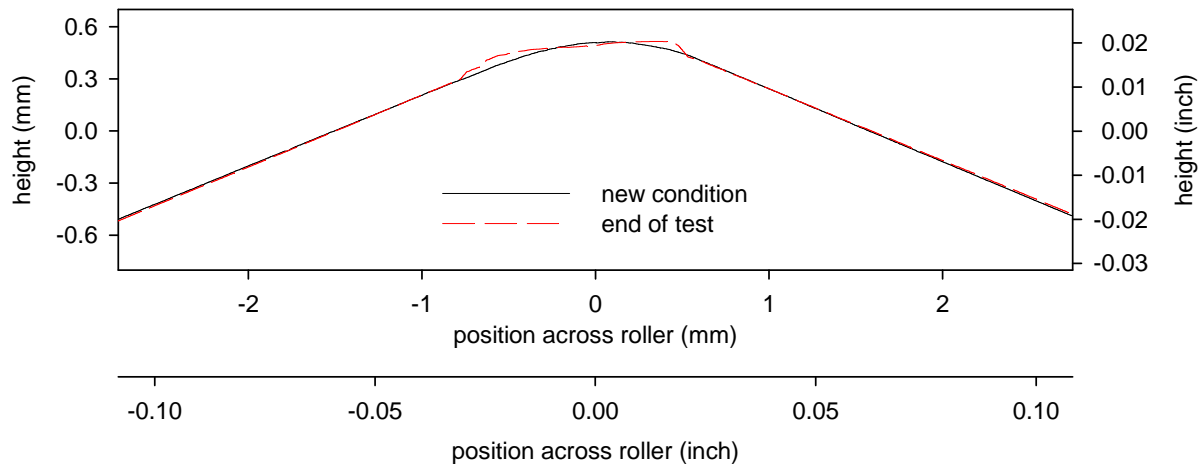


Figure 28.—Profile trace of the blend radius geometry roller when new and after testing, plotted using true aspect ratio to show the shape of the geometry.

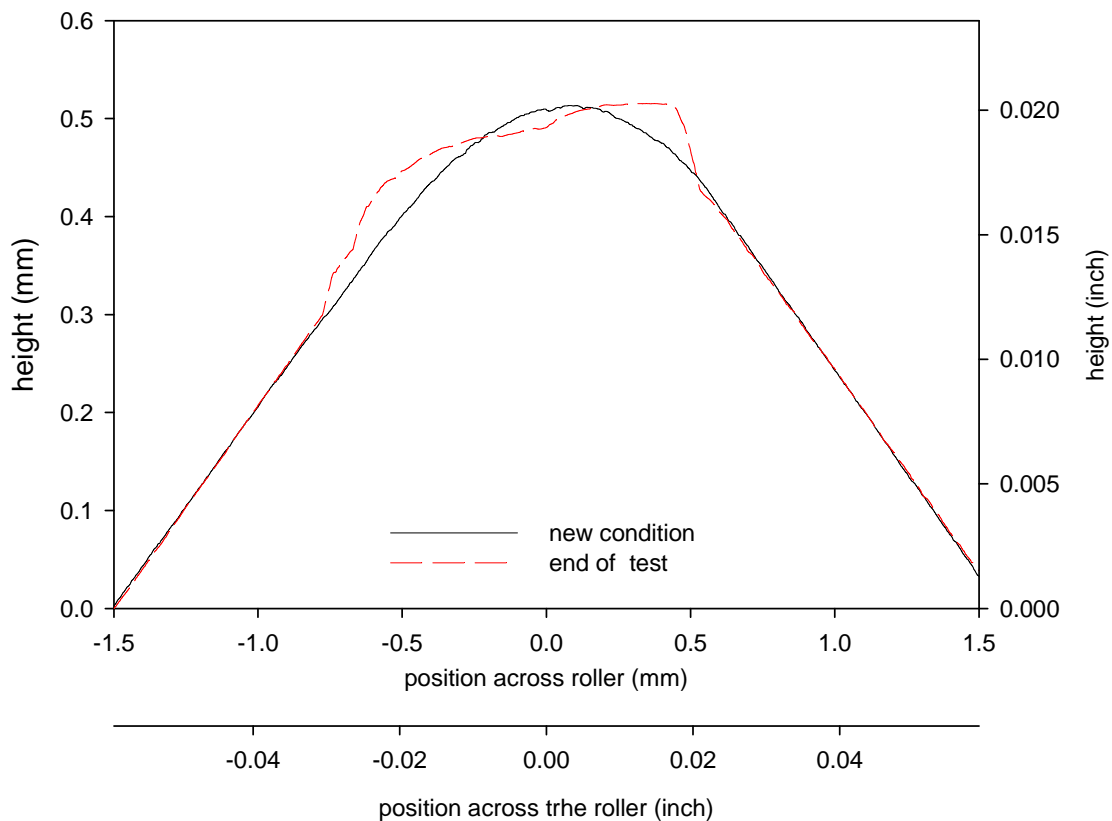


Figure 29.—Profile trace of the blend radius geometry roller when new and after testing, plotted using expanded ordinate scale to show detail.

The damage initiation test described herein demonstrates a plausible scenario for the damage of the SARJ ring. The geometry of the SARJ rollers includes a blend radius for transition from the nominally flat profile to the 45° chamfer geometry. Traction forces that develop from even small values (within specification) of shaft misalignment and moderate friction capacity of the contact from inadequate lubrication shifts the contact pressure from the nominally designed condition. For such a condition, at least some of the normal load is carried on the blend radius geometry region. The test demonstrated that high concentrations of the normal load and traction force onto the blend-radius geometry can compromise the nitrided surface within a very low number of shaft revolutions. The debris and damaged surface of test roller has features that match the SARJ hardware. We considered the damage initiation testing as being representative of the damage that occurred to the SARJ ring. The damaged test roller was then used for additional damage propagation and durability testing.

Results of Damage Propagation Testing

To propagate the damage initiated on the nitrided 15-5 test roller and mimic the damage observed on the SARJ ring, damage propagation testing was completed. The damage propagation testing was completed in 1 test session using a single load step of 907 N. The nitrided roller with damage initiation was mated with a new-condition 440C roller having an 81 mm crown radius. No lubrication was used for the damage propagation testing. A vacuum was established before starting the test. The test conditions used are provided in Table 2. The Hertz pressures reported in Table 2 are the pressures that would be obtained if both rollers were undamaged and perfectly smooth. As was presented in Figure 17, the actual contact pressures are significantly different from these calculated values via Hertz analysis. However, these Hertz contact pressure values provide a means for quantifying the load intensity relative to the SARJ mechanism.

The condition of the rollers could be assessed visually through a window of the test chamber. Damage propagation and debris generation began as soon as the test started. From visual assessment during the test operations, the level of damage progression was fairly constant and continuous throughout the testing. The testing was completed when the extent and severity of damaged was judged as similar to the compromised SARJ race ring.

The axial force on the test roller was measured, and the data is provided in Figure 30. During testing the axial force quickly increased to a value of about 300~350 N during the first 2000 shaft revolutions and axial force was highly variable. After about 2000 shaft revolutions the axial force averaged about 290 N (or 0.32 times the normal load) and had less variation as compared to the first 2000 shaft revolutions.

The visual appearances of the nitrided roller after completion of the damage propagation testing for three different orientations about the periphery are provided in Figures 31 to 33. The region depicted in Figure 31 is the region where the initial chip liberated during the damage initiation testing. Islands of material remain surrounded by missing material. It appears that several large chips were liberated from this region of the roller. The region depicted in Figure 32 suggest a variety of damage mechanisms including plastic deformation of asperity features, chipping-like fractures, and over-rolling of chipped debris. There may also be some material transfer from the mating roller. The region of Figure 33 includes a ragged edge with a sharp slope suggesting a very sudden transition from the nitrided roller surface to the depth where the core (un-nitrided) material is present.

TABLE 2.—TEST CONDITIONS FOR THE DAMAGE PROPAGATION TESTING

Step	Load (N)	Max. Hertz Pressure (GPa)	Mean Hertz Pressure (GPa)	Speed (rpm)	Misalignment (degrees)	Cycles
1	907	1.7	1.1	20	0.7	5580

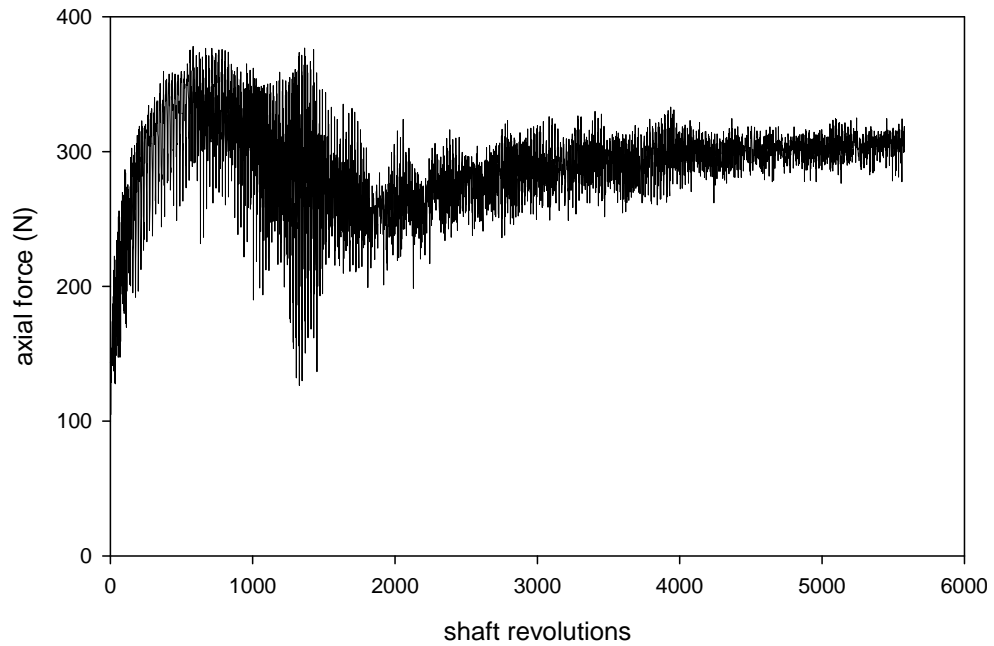


Figure 30.—Trend of the measure axial force as a function of shaft revolutions during the damage propagation testing.



Figure 31.—Condition of the nitrided roller after the damage propagation test, circumferential location 1.



Figure 32.—Condition of the nitrided roller after the damage propagation test, circumferential location 2.



Figure 33.—Condition of the nitrided roller after the damage propagation test, circumferential location 3.

To inspect the depth of the roller damage, a set of stylus profilometer inspections were completed. The nitrided roller was inspected at eight circumferential locations of approximately equal spacing around the periphery. The plots also include the inspection data after damage initiation for easy comparison. Results from selected positions will be discussed as follows. The inspection data at the location where the initial chip was liberated (location #7) is provided in Figure 34. Both after damage initiation and after damage propagation, the depth of the material removed is to approximately equal to the thickness of the nitrided layer (depth of 15 μm). The main effect of the damage propagation testing was to extend the region where material is fractured and/or worn away while the maximum depth of the material removed did not increase significantly. The same effect of extending the region of material removal limited to a depth of about 15 μm is evident at all circumferential locations including location #2 (Fig. 35) and location #5 (Fig. 36). Figure 37 provides results of profilometer inspections of the 440C roller after completion of the damage propagation test. The roller surface has been roughened, but it appears that material was not lost in any significant volume. In fact, the inspection suggests added material which could be by cold-welding or by overrunning and compacting of loose debris from the mating nitrided roller.

The total mass loss from the nitrided roller after the damage propagation testing was about 0.29 grams. The mass of the nitrided layer across the working region of the roller face is approximately 0.9~1.0 grams of material. The plots of Figures 34 to 36 show that approximately 1/3 of the nitrided layer has been removed from the working face of the roller by the combined damage initiation and damage propagation testing.

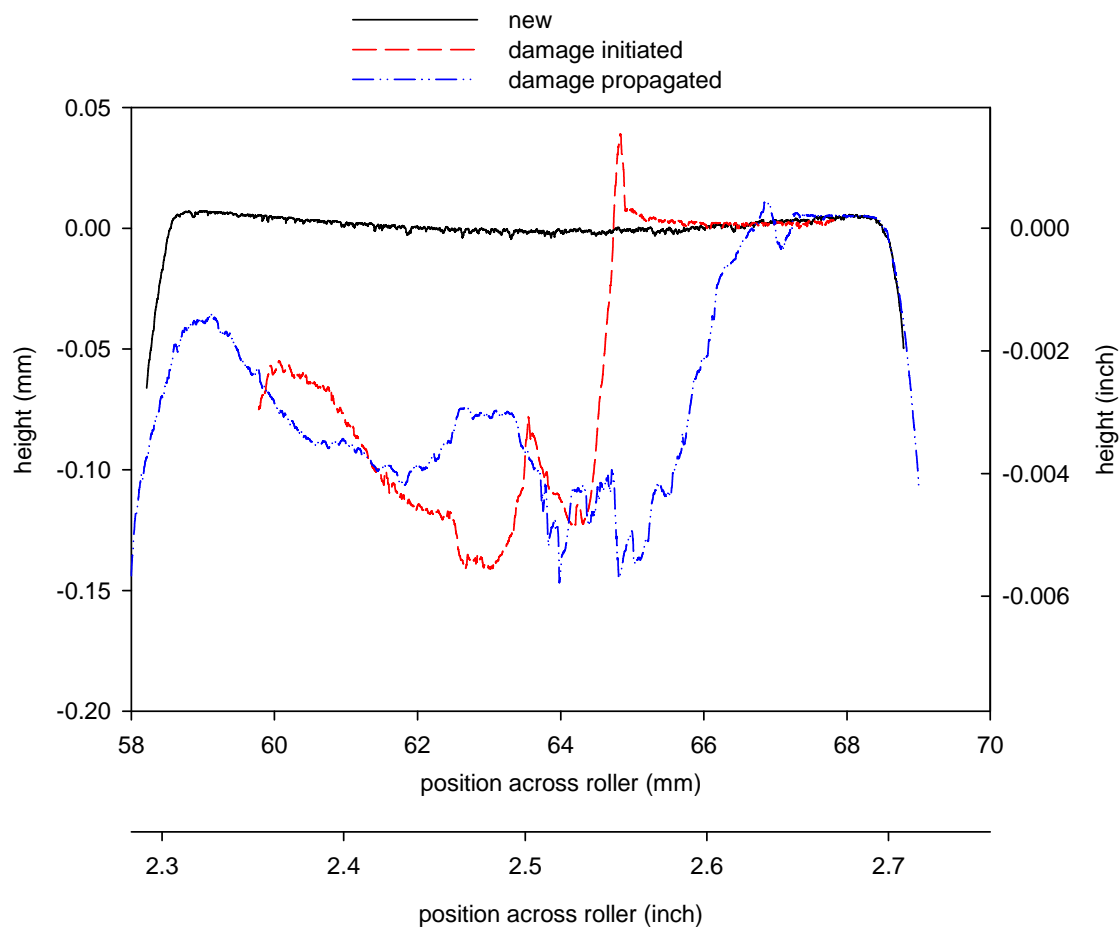


Figure 34.—Profile traces across the roller width documenting the new condition, condition after damage initiation testing, and condition after damage propagation testing, circumferential position #7.

The damage propagation test described herein demonstrates a plausible scenario for the damage of the SARJ ring. The damaged surface of the test roller has features that match the SARJ hardware. Each SARJ ring working surface interacts with 16 rollers, and each roller will impose a different contact pressure profile depending on the misalignment angle direction and magnitude. However, once the nitride layer is compromised the main effect will be a bridging of the damaged regions similar to the manner of the test roller (Fig. 17). Using the cycle counting approach described earlier in this document, the 5580 cycle damage propagation test represents about three weeks of SARJ operation time. The test demonstrated that extensive damage propagation can occur with relatively few cycles. We considered the damage initiation and damage propagation testing as being representative of the damage that occurred to the SARJ ring. The damaged test roller was then used for additional durability testing.

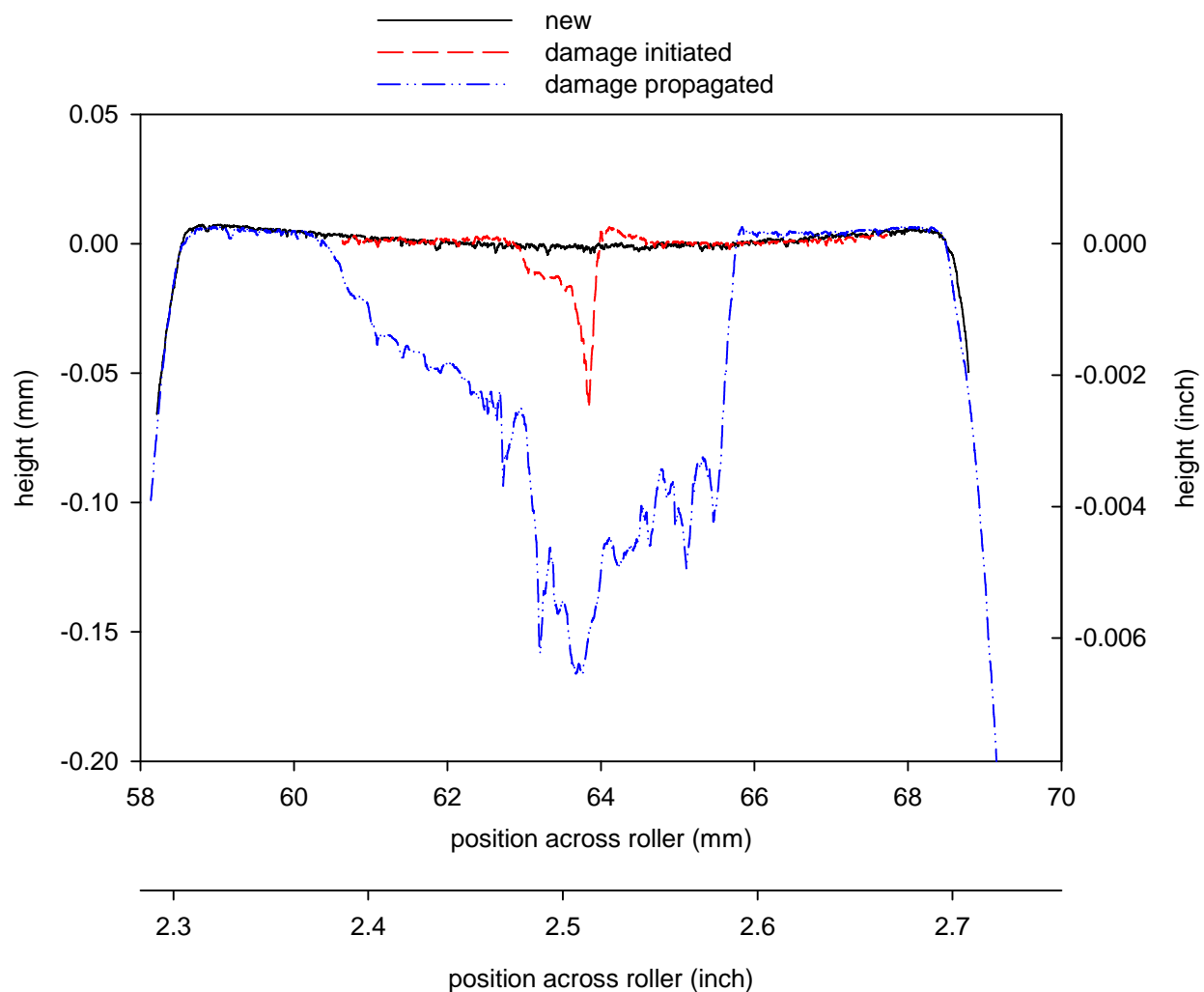


Figure 35.—Profile traces across the roller width documenting the new condition, condition after damage initiation testing, and condition after damage propagation testing, circumferential position #2.

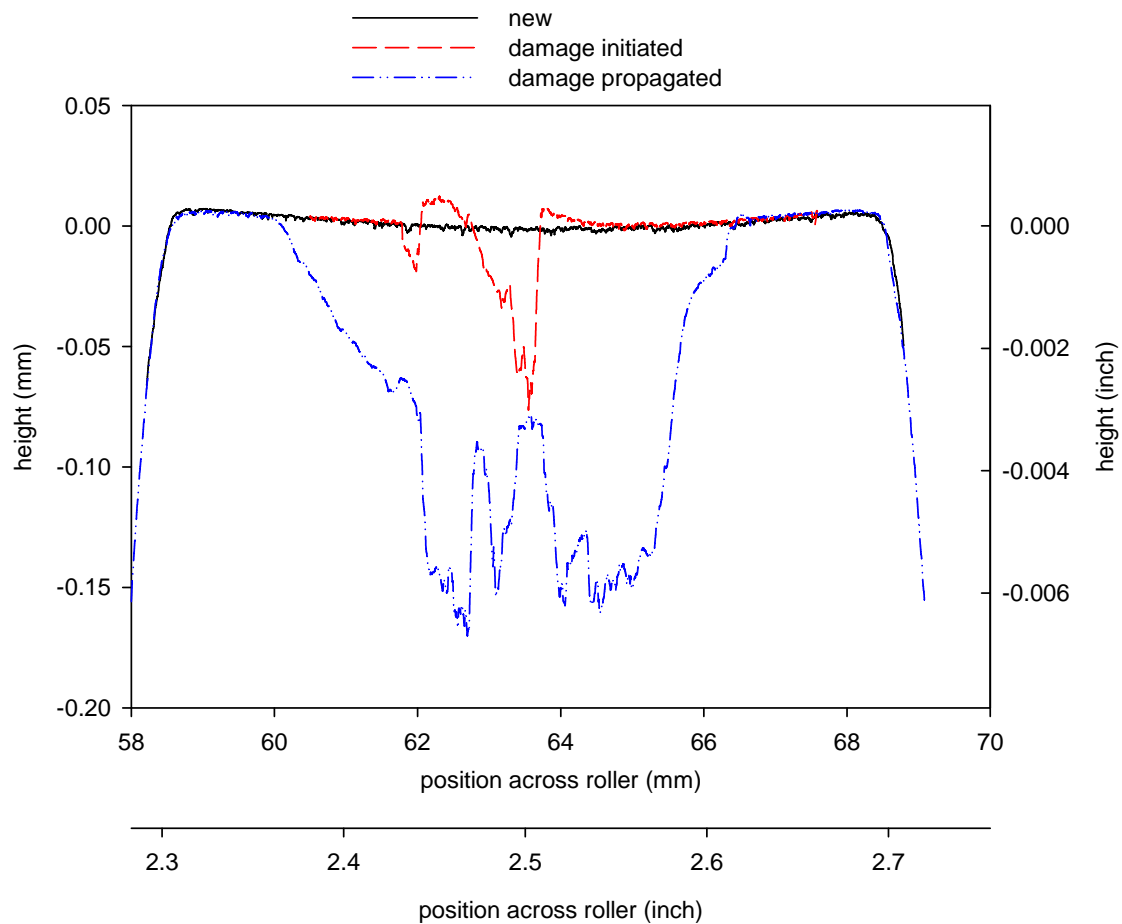


Figure 36.—Profile traces across the roller width documenting the new condition, condition after damage initiation testing, and condition after damage propagation testing, circumferential position #2.

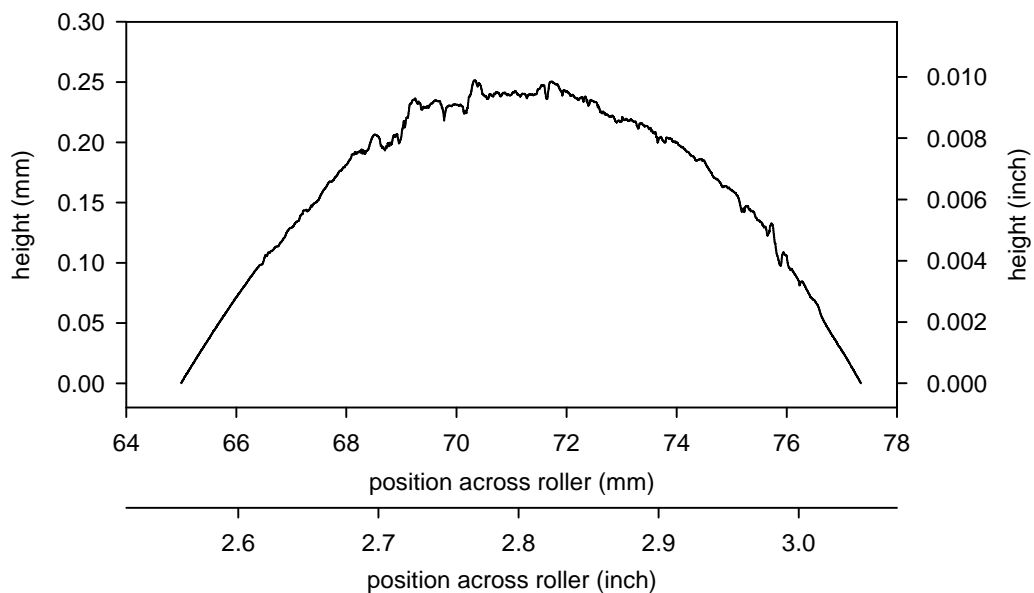


Figure 37.—Profile of the 440C roller at end of the damage propagation testing.

Results of Roller Durability Testing

Durability Test Operations Summary

To study the durability of the compromised nitrided 15-5 SARJ ring, a durability test was completed using the damaged 15-5 test roller. The damaged roller was mated with a new-condition 440C roller having an 80.5 mm (3.17 in.) crown radius. The testing was done over many sessions, each session lasting a single working day since the rig was not equipped for unattended, around-the-clock operation. A vacuum of about 5×10^{-6} torr was established before starting a test increment. The test chamber was isolated in-between testing sessions, and a vacuum of about 50×10^{-3} torr was maintained. The chamber was opened as needed to apply grease (re-lubrication) and/or for roller removal for detailed inspections. For purposes of reporting the testing herein, the testing is summarized by a testing interval. A new test interval was established by a re-greasing action. The durability test comprised of sixteen testing intervals. Each test interval included two or more working day test sessions. The operating conditions used for all test intervals are provided in Table 3. The rationale for selecting the operating conditions was previously summarized in the “*Test Conditions to Study Roller Durability*” section of this document.

TABLE 3.—OPERATING CONDITIONS FOR THE ROLLER DURABILITY TESTING

Interval	Normal load (N)	Max. Hertz pressure (GPa)	Mean Hertz pressure (GPa)	Cycles (incremental)	Cycles (accumulated)	Reason to re-grease	Speed (rpm)
1	947	1.7	1.1	7,416	7,416	high traction	5.8
2	979	1.7	1.1	11,007	18,423	collect debris	5.8
3	970	1.7	1.1	7,441	25,864	collect debris	5.8
4	770	1.6	1.1	81,887	107,751	collect debris	80
5	787	1.6	1.1	113,465	221,216	high traction and debris	65
6	774	1.6	1.1	186,298	407,514	2-year equivalent interval	79
7	770	1.6	1.1	85,443	492,957	collect debris	80
8	801	1.6	1.1	101,849	594,806	moderate traction	81
9	765	1.6	1.1	124,962	719,768	debris noticed	79
10	734	1.6	1.0	112,706	832,474	traces of debris	80
11	725	1.6	1.0	162,345	994,819	high, steady traction	79
12	747	1.6	1.1	103,978	1,098,797	high traction	79
13	765	1.6	1.1	77,958	1,176,755	cycle of 2 testing days	80
14	778	1.6	1.1	58,092	1,234,847	cycle of 2 testing days	79
15	774	1.6	1.1	79,682	1,314,529	cycle of 2 testing days	80
16	787	1.6	1.1	78,000	1,392,529	cycle of 2 testing days	80

Note: Misalignment angle was -0.7° for all test intervals.

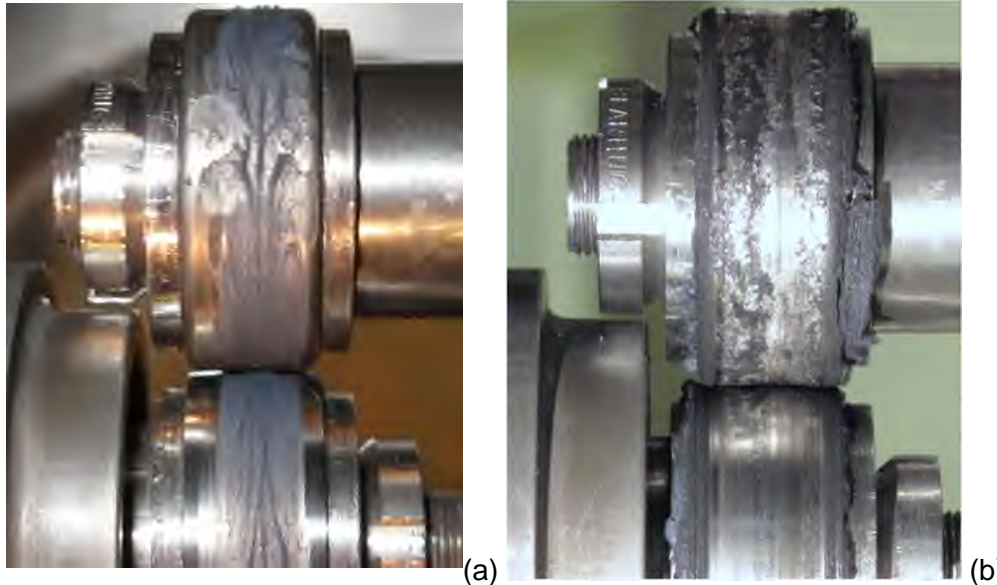


Figure 38.—Typical view of test rollers during a re-greasing action. (a) View after application of grease. (b) View of the same rollers at end of a testing interval.

Figure 38 shows the typical appearance of test rollers at the start and end of a testing interval. Figure 38(a) shows the rollers with an application of grease distributed by rotating the rollers with a very small gap between the two surfaces. Figure 38(b) shows the rollers after completion of a testing interval. The grease becomes displaced out of the contact to the sides of the rollers. It was difficult to determine the expected traction condition (lubrication effectiveness) based solely on a visual assessment through the chamber viewing window. Surface that appeared depleted of grease could still maintain a low level of traction for some time, but eventually a re-greasing was judged needed based on the appearance of significant wear debris and/or a steady and high magnitude of the axial force.

Visual Assessments of Surface Conditions

The rollers were removed from the test rig for detailed inspections several times. Figures 39 to 45 show views of the roller surfaces at intervals of approximately 0.03, 0.41, and 1.39 million durability cycles. Figures 39 to 41 provide overall views of the nitrided 15-5 roller, and Figures 42 to 44 provide magnified views of the nitrided roller surface. These images show the evolution of the surface damage. The extent of damage after even only 25,864 cycles (Fig. 39) is significantly greater than the beginning of the durability test (Figs. 31 and 32). After 407,514 durability cycles the damage has progressed to cover most of the roller surface (Fig. 40). Although the grease lubrication will provide some wear protection, the compromised nitrided surface layer continues to crumble away in a fairly rapid fashion. The damage processes over the first 400,000 cycles appear to be a combination of brittle fracture by overload, plastic deformation, and over-rolling of debris. The surfaces of the rollers after completion of the test (1.39 million durability cycles) suggest that the fracturing process became completed, and the surface at the end of the test appears to be affected by continued abrasive wear, over-rolling and compacting of debris, and localized plastic deformation. The condition of the mating 440C roller is documented by the images of Figure 45. The 440C roller surface has some shallow grooving during the earlier test intervals (Figs. 45(a) and (b)) when the mating 15-5 roller still had a partial nitride layer surface that is hard and abrasive. At the end of the test (Figs. 45(c) and (d)) the 440C surface was smoothed somewhat, but appears to have been worn to some depth by abrasive wear.

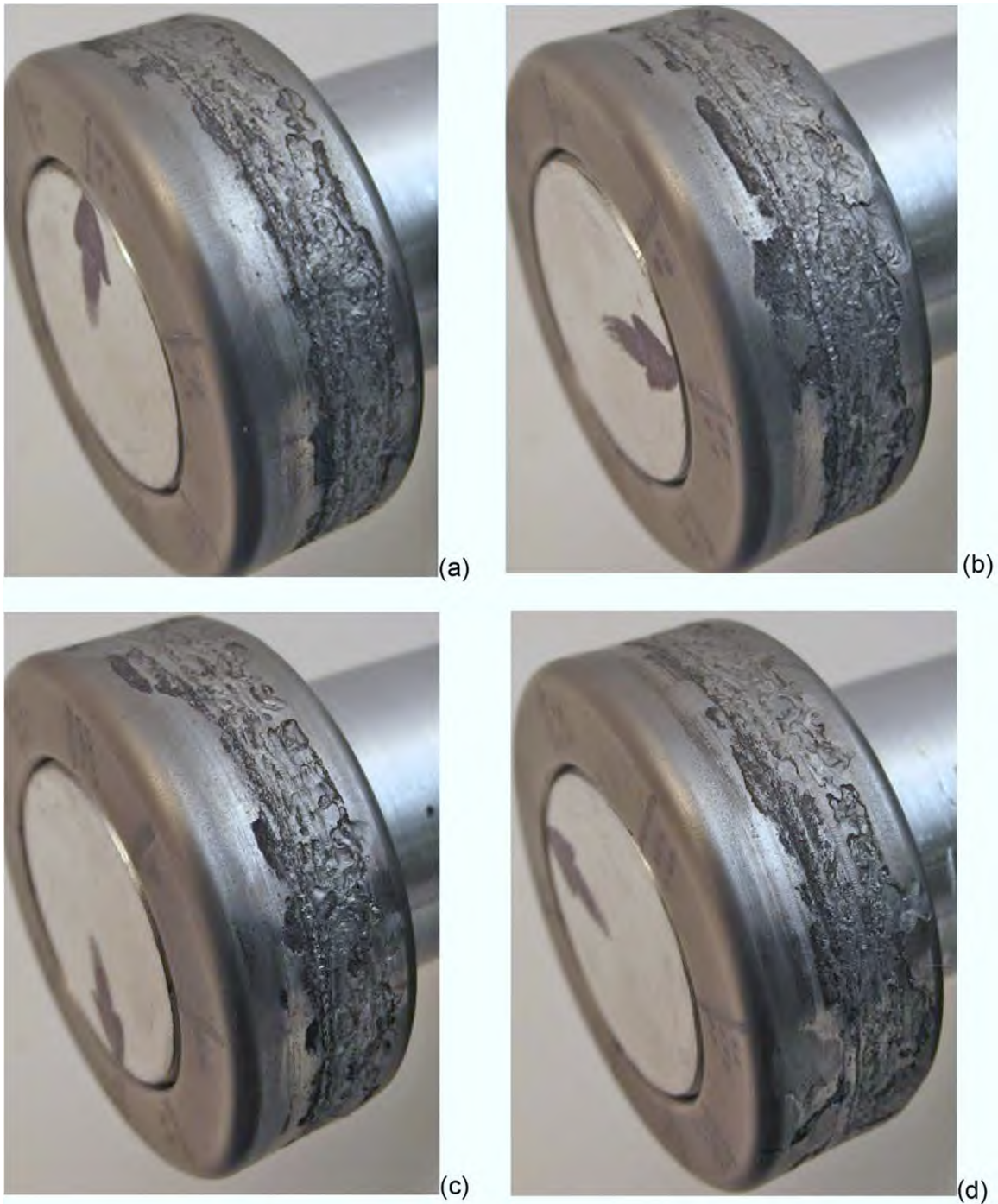


Figure 39.—Condition of nitrided 15-5 roller after completion of durability test interval 3 (25,864 durability cycles). Views (a) to (d) are sequentially rotated 90° per arrow mark on end of shaft.

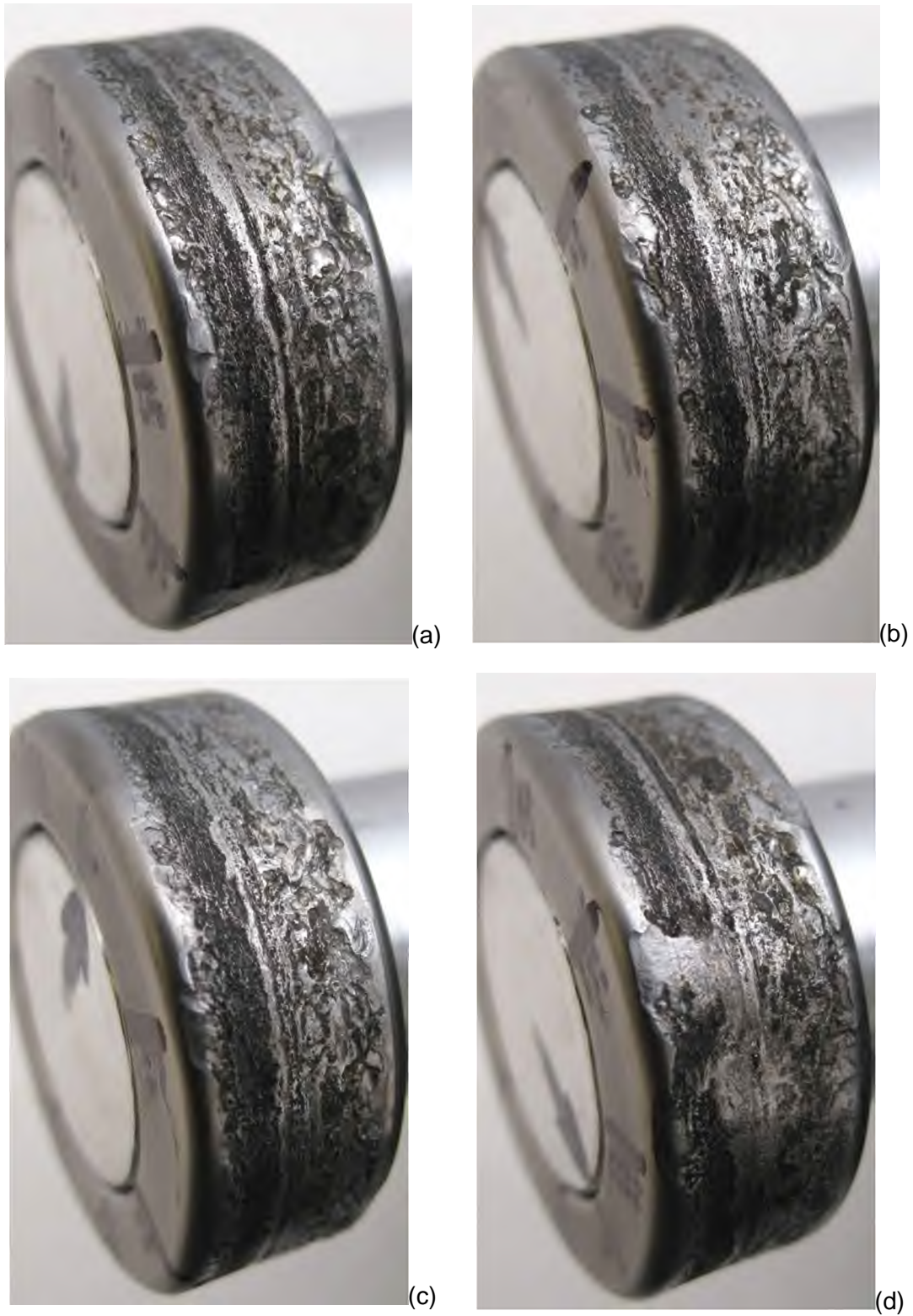


Figure 40.—Condition of nitrided 15-5 roller after completion of durability test interval 6 (407,514 durability cycles). Views (a) to (d) are sequentially rotated 90° per arrow mark on end of shaft.

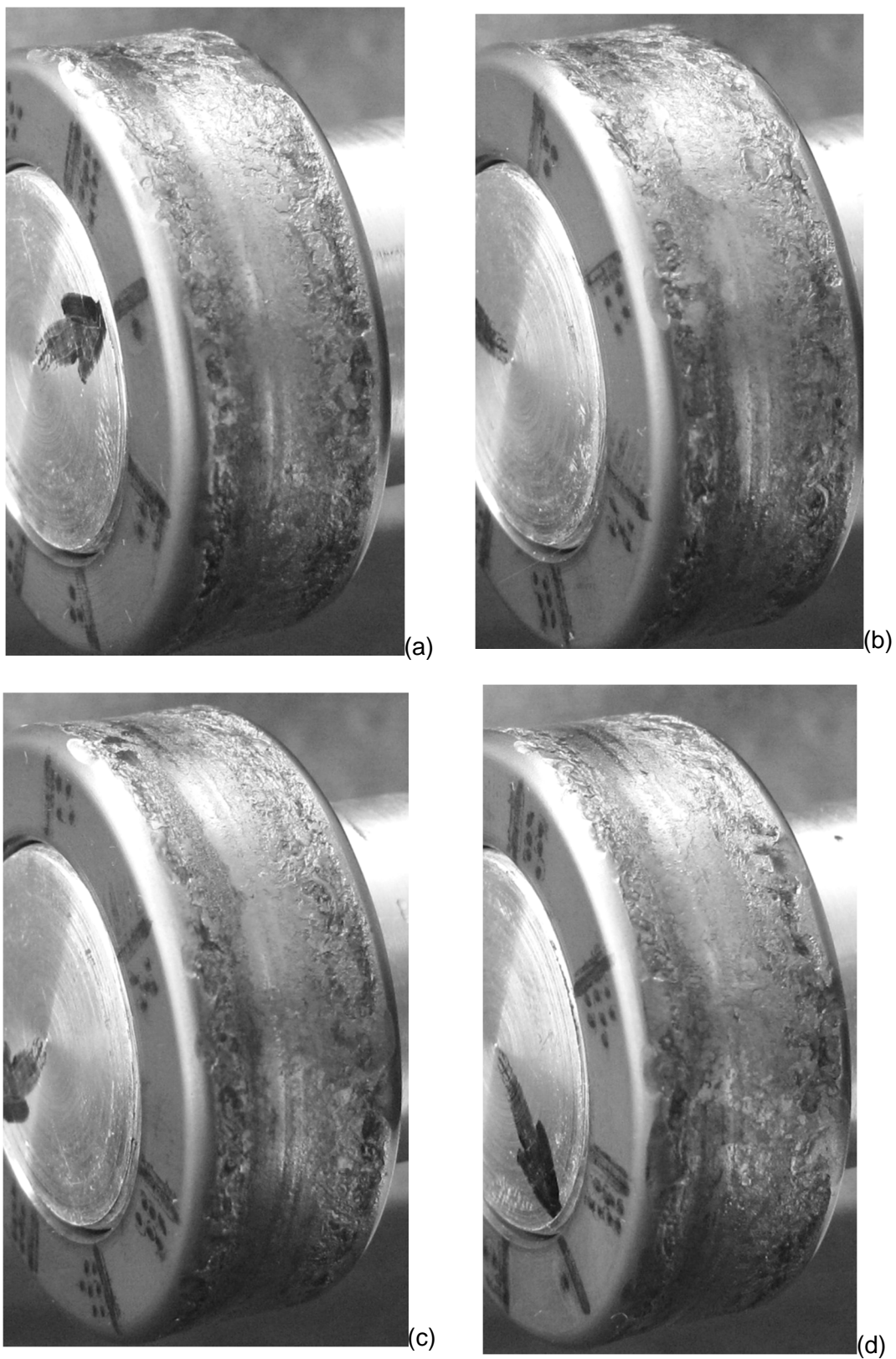


Figure 41.—Condition of rollers after completion of durability test (1.39 million durability cycles). Views (a) to (d) are sequentially rotated 90° per arrow mark on end of shaft.

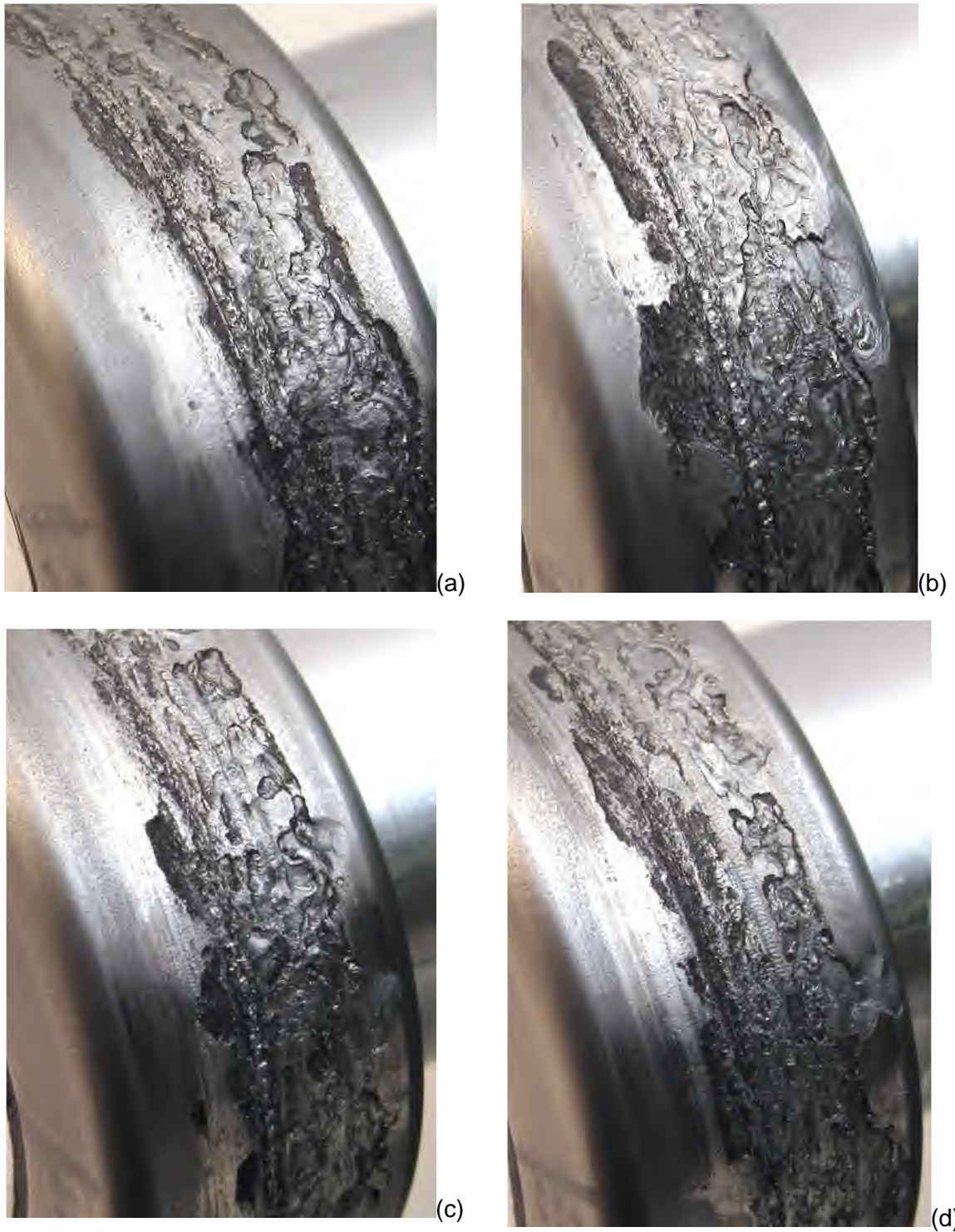


Figure 42.—Condition of nitrided 15-5 roller after completion of durability test interval 3 (25,864 durability cycles). Views (a) to (d) are sequentially rotated 90° as Figure 39 but with magnified view of details.

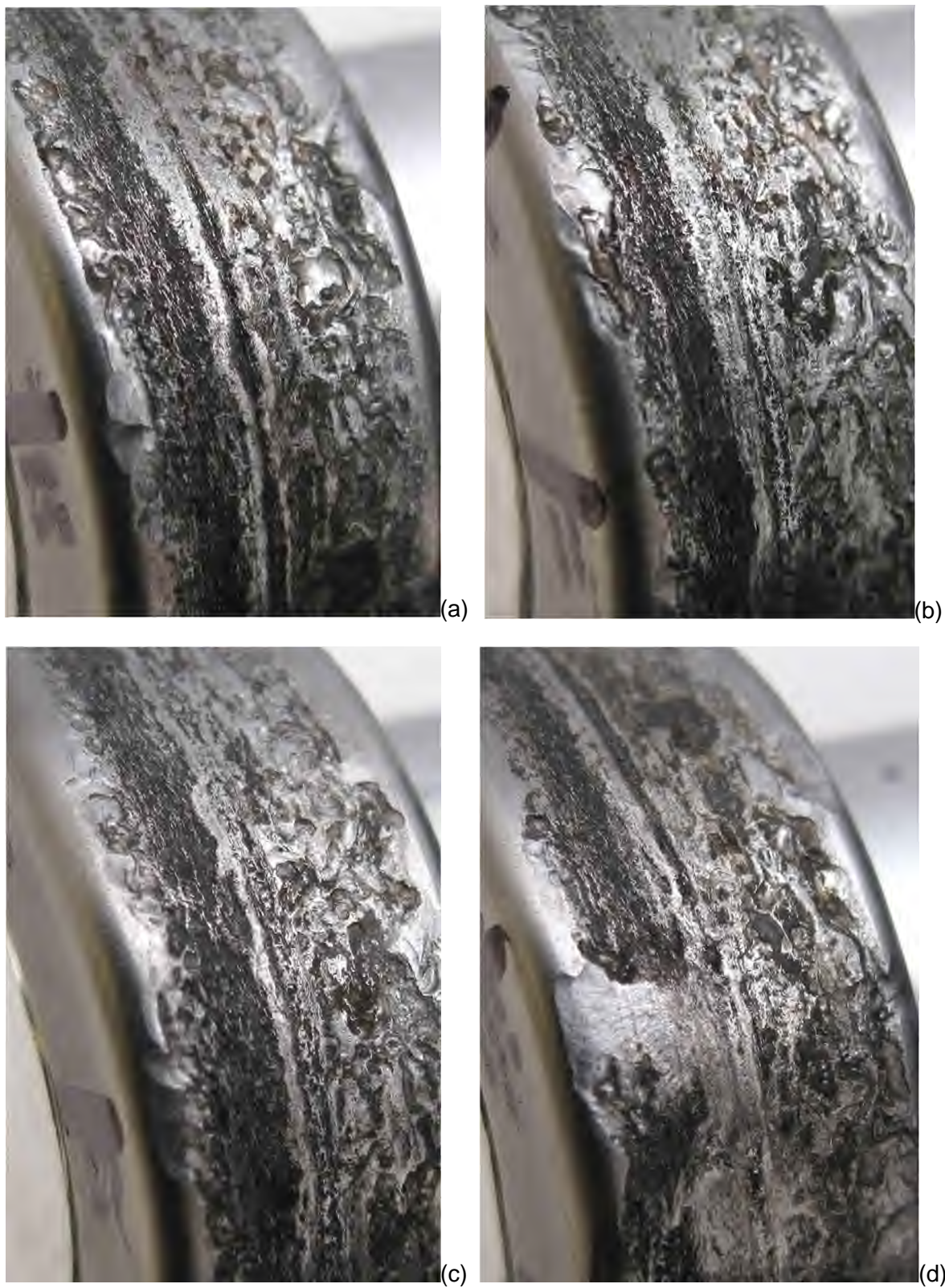


Figure 43.—Condition of nitrided 15-5 roller after completion of durability test interval 6 (407,514 durability cycles). Views (a) to (d) are sequentially rotated 90° as in Figure 40 but with magnified view of details.

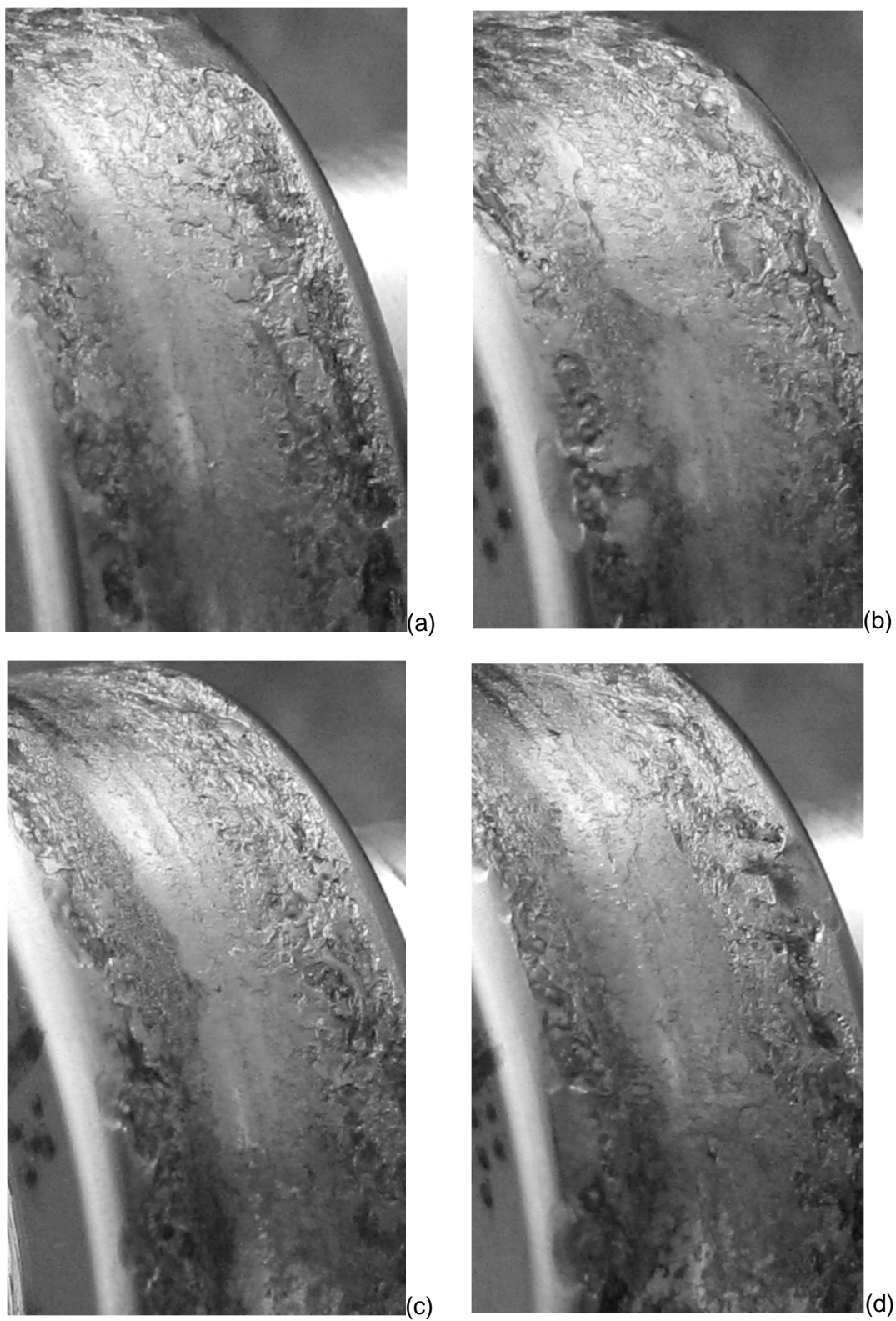


Figure 44.—Condition of nitrided 15-5 roller after completion of durability test (1.39 million durability cycles). Views (a) to (d) are sequentially rotated 90° as in Figure 41 but with magnified view of details.



(a)



(b)



(c)



(d)

Figure 45.—Condition of 440C roller at intervals of durability test: (a) end of interval 3 (25,864 cycles), (b) end of interval 6 (407,514 cycles), (c) end of test (1.39 million cycles), (d) end of test, magnified view.

TABLE 4.—CHANGES OF MASS OF TEST ROLLERS

			nitrided 15-5 roller # N4	440C mating rollers
		cycles	change in mass (grams)	
no grease	damage initiation	3,544	- 0.07	+ 0.02
	damage propagation	5,580	- 0.29	not recorded
with grease	durability	407,514	- 0.94	- 0.09
		1,392,529	- 1.20	- 0.20

Mass Change of Rollers

The mass change of the rollers was tracked at several intervals. Table 4 provides a summary of the mass change data. The change in mass listed is the accumulated total mass change. The total mass loss from the nitrided 15-5 roller at the end of the durability test was 1.2 grams. Of the total mass lost during the durability testing, about 70 percent of the loss occurred during the first 30 percent of the durability test. The mass of the nitrided layer covering the working surface of the test roller was estimated as 0.9~1.0 grams. The mass loss of 0.94 grams after completion of 407,514 durability cycles suggests that most of the nitride layer has been removed at that time. From the visual assessment of the surface conditions it appeared that during the earlier part of the durability test the wear process was dominated by brittle fracture and overload failures of the compromised nitrided layer. During the later stages of the durability test the wear process was more dominated by a continuous abrasive wear process. The mass loss rate was greater during the earlier stages of the durability testing. The mass loss from the mating 440C roller was at a lesser rate than the 15-5 roller, as would be expected since the 440C roller is harder than is the core 15-5 roller material that was exposed during the later stages of the durability test.

Profilometer Inspections of the Tested Rollers

The test rollers were removed from the test rig several times for detailed inspections including inspection via a stylus profilometer. The rollers were traced across the roller working surface in the axial direction. The circumferential positions where the axial profile traces were collected were tracked by markings on the sides of the rollers. The nitrided roller was inspected at eight circumferential positions. The mating 440C roller was more uniform about the circumference and so was inspected at only three locations. Profile traces were overlaid by matching up portions of the data traces from the unworn parts of the roller. The overlaying was done manually by subjective judgment to shift the traces along the ordinate and abscissa. In some cases, the relative positioning could be done with a high confidence because there was sufficient data from unworn regions of the roller. In other cases the worn and damaged regions were extensive enough that overlaying could not be accomplished with confidence. Plots and discussion of data from two circumferential positions illustrating typical results follow below.

Figures 46 and 47 are plots of profilometer data for the nitrided 15-5 test roller at circumferential positions #1 and #4, respectively. The data for the damage initiation and propagation testing done before application of grease are provided for comparison. Note that during the first 25,864 cycles of the durability test with grease, the main effect seems to be an extension of the damage to the nitride layer extending the damage in the region where the groove into the nitride layer has the steepest slope. After 407,504 durability cycles, the damage had become extended over most of the active width of the roller. The damaged region includes some sharp slopes through the middle region of the profile. At this stage of

the testing the damage is for the most part confined to a depth of the nitrided material. After 1.39 million durability cycles the wear and damage has extended to the entire width of the roller. The center portion of the profile now has a relatively smooth surface and more gentle slopes as compared to earlier intervals. The wear depth may now have penetrated somewhat beyond the depth of the nitrided material into the un-nitrided core material. Based on the relative volumes of material removed, the details of the profile traces, and the visual appearance of the surfaces it is apparent that the dominant degradation mechanism changed over the duration of the testing. During the earlier intervals the nitrided layer fractured away. During the later intervals core material wore via abrasive wear.

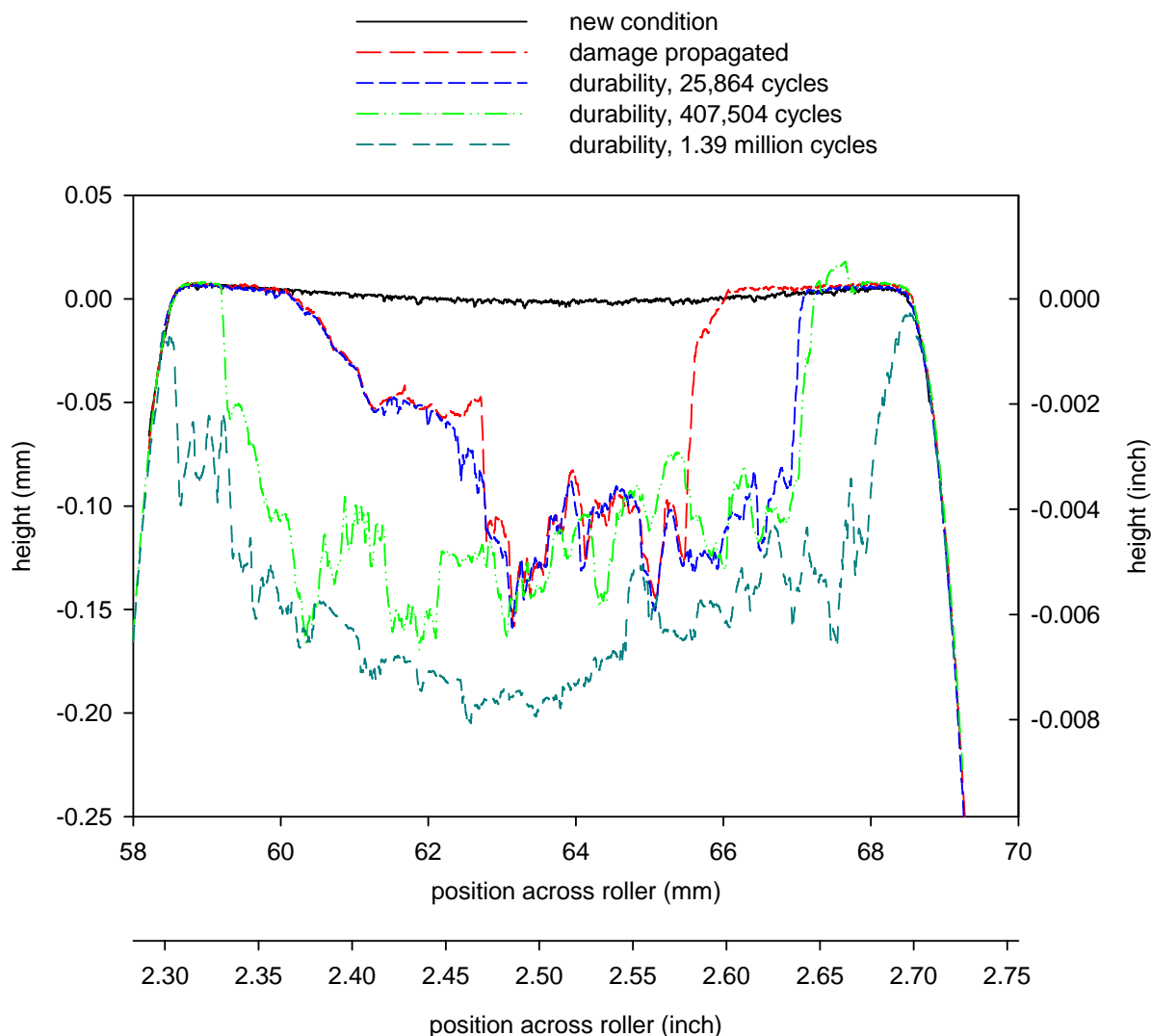


Figure 46.—Profile inspections of the nitrided 15-5 roller at circumferential position #1.

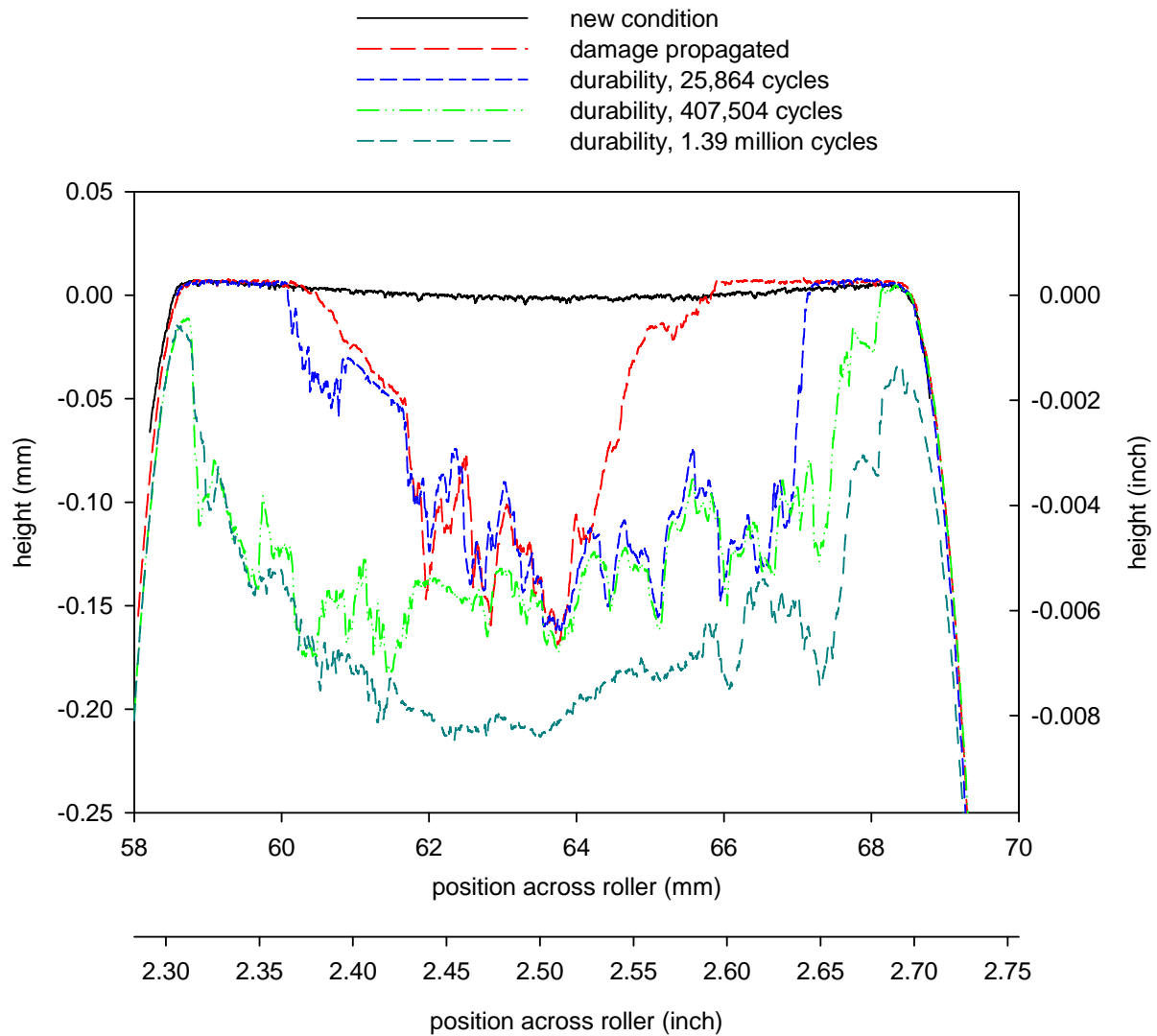


Figure 47.—Profile inspections of the nitrided 15-5 roller at circumferential position #4.

Figures 48 and 49 are two plots of profilometer data for the 440C roller. Figure 48 is a raw data trace of the crowned roller. The data of Figure 49 was calculated from the data of Figure 48 using a least-square fit procedure to remove the original crown form of the data idealized as an arc of known radius calculated from a trace of roller before testing. The depth of wear on the 440C roller is about 15 to 25 percent of the wear depths for the mating nitrided roller. Based on both the profile data and the visual appearance of the tested surface, the primary wear mechanisms appear to be mild abrasive wear along with some asperity-scale galling.

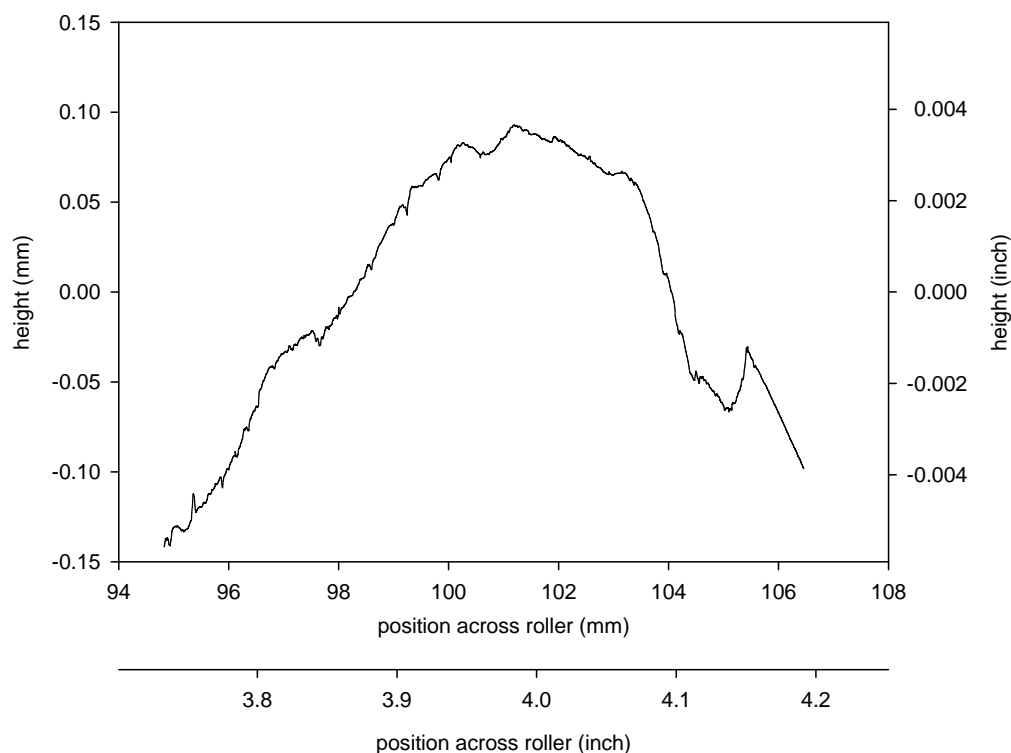


Figure 48.—Profilometer inspection of the 440C roller at the end of the durability test.

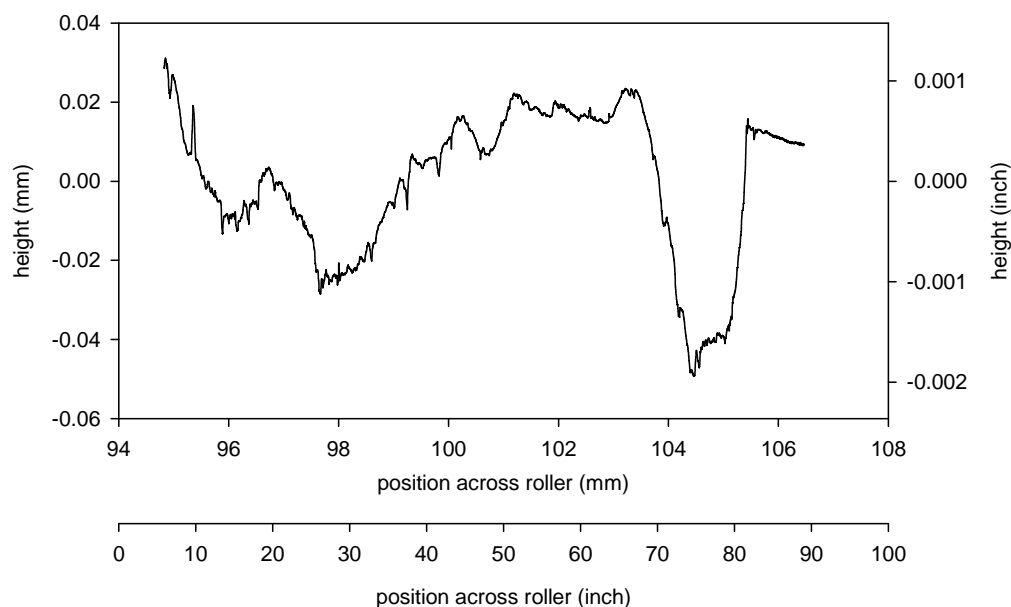


Figure 49.—Profilometer data for the 440C roller at the end of the durability test after removal of arc by least-squares best fit.

Axial Force Measurements

The force created by the shaft misalignment and traction condition was measured during testing. The force is termed herein the axial force as it is directed in the direction of the roller rotational axis. Trends of the axial force as a function of shaft revolutions during four different stages of the durability testing are provided in Figures 50 to 53. The intervals mentioned in the figure titles and discussion to follow refer to the re-lubrication intervals as listed previously (Table 3).

Figure 50 provides the trend of the axial force normalized to the normal force as a function of shaft revolutions for test interval #3. This testing interval comprised three working day sessions and a total of 7441 shaft revolutions. The operating speed was 5.8 rev/min. The axial force was limited to about 0.15 times the normal load. For the shaft misalignment angle of 0.7° used for the durability testing, previous experiments have demonstrated that dry (unlubricated) rollers of these materials could generate an axial force of about 0.4 times the normal force. Therefore, the contact appears to be well lubricated throughout test interval #3. Test interval #3 was completed and a re-lubrication action was taken based on the amount of debris that was generated. During this part of the durability testing debris was likely generated by localized overloading of the nitride layer at the edges of the damage track (overloading per contact pressure profile, Fig. 17). While the lubrication proved effective for the long-term durability, the compromised nitride layer continued to fracture away in spite of the grease lubrication.

Figure 51 provides the trend of the axial force normalized to the normal force as a function of shaft revolutions for test interval #4. The operating speed was increased from the 5.8 rev/min used for interval #3 to 80 rev/min for interval #4 to accelerate the durability testing. A fresh application of grease was applied before the start of test interval #4. The testing was complete over two working day sessions comprising 81,887 shaft revolutions. The SARJ ring material will experience this number of roller contact stress cycles over 10.7 month of continuous operation. The speed appears to have some influence on the level of axial force that can develop as the force is much higher than recorded during the preceding interval #3. The large variation of the axial force perhaps represents the release of strain energy as the nitride layer fractures into small fragments of debris. The test interval was interrupted for re-lubrication based on the volume of debris generated.

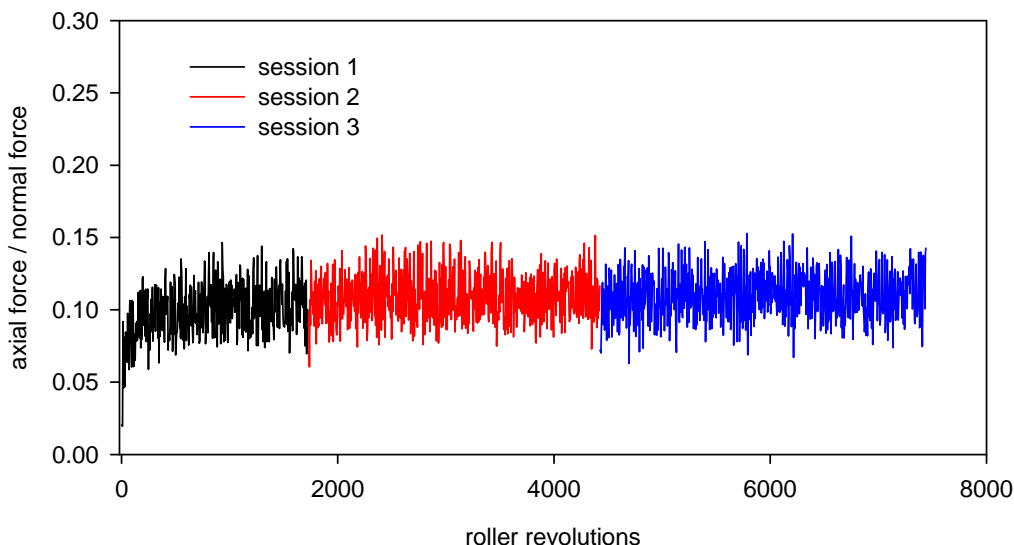


Figure 50.—Trend of thrust load to normal load ratio during testing interval #3 comprising 7,441 roller evolutions.

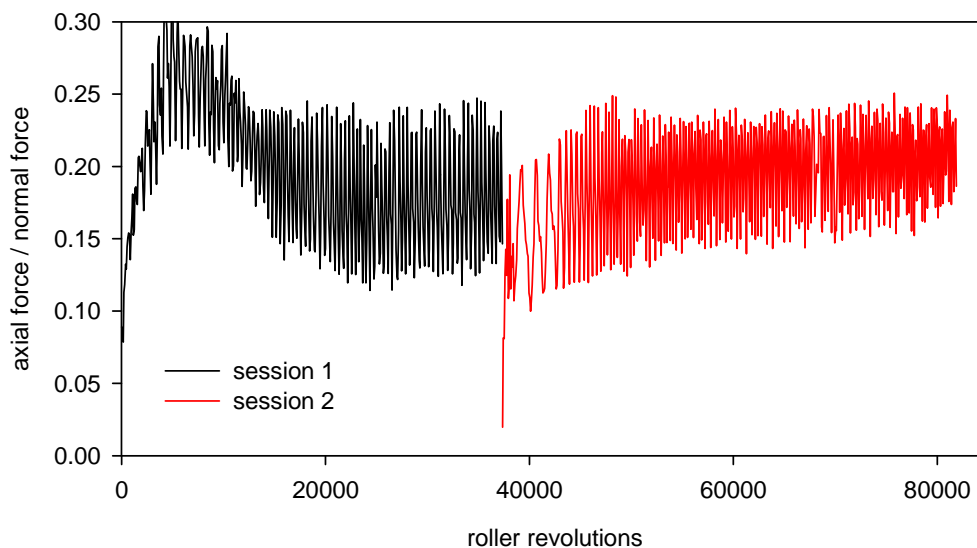


Figure 51.—Trend of thrust load to normal load ratio during testing interval #4 comprising 81,887 roller revolutions.

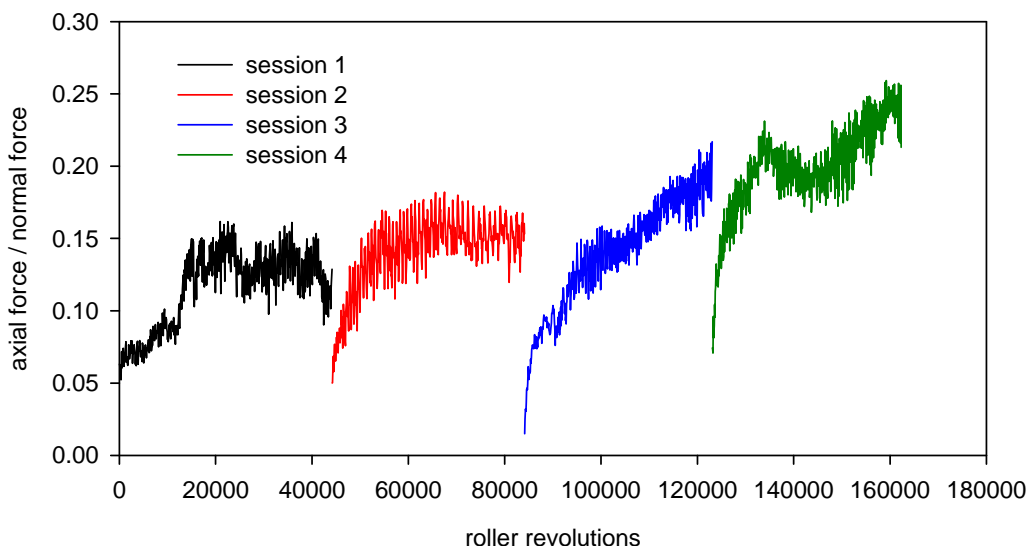


Figure 52.—Trend of thrust load to normal load ratio during testing interval #11 comprising 162,345 roller revolutions.

Figure 52 provides the trend of the axial force normalized to the normal force as a function of shaft revolutions for test interval #11. The operating speed during this test interval was 80 rev/min. The testing was completed over 4 working-day sessions comprising a total of 162,345 shaft revolutions representing about 21 months of continuous SARJ operation. At this juncture of the durability test the volume of debris generated was greatly reduced as compared to the early test intervals. The axial force value has a steady increasing trend as the grease becomes less effective. When the rig operation was interrupted at the end of a working day session and restarted the next day, the axial force was low when the rig was restarted and then would increase back to the magnitude experienced the previous day. The rate at which the axial force increases seems to be related to and is an indicator of the lubrication effectiveness. It is proposed that the idle time at the end of a test session until a restart the next morning might allow for the oil from the grease to reflow into the contact providing for some time a more effective lubrication condition. The testing interval was completed and a re-greasing chosen based on the steadily high axial force at the end of session #4.

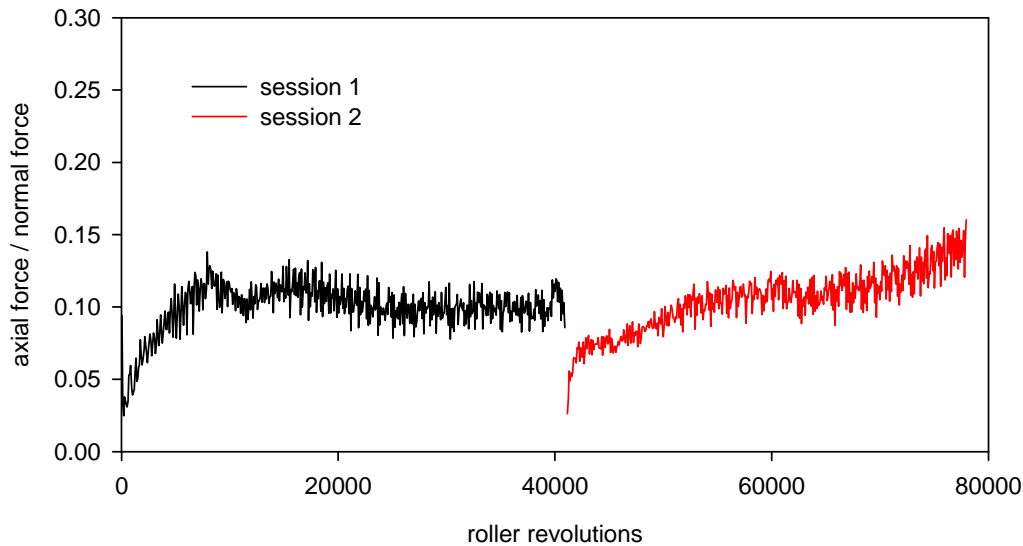


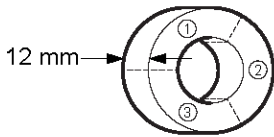
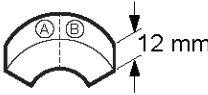
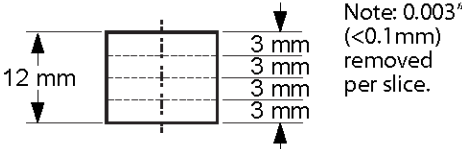
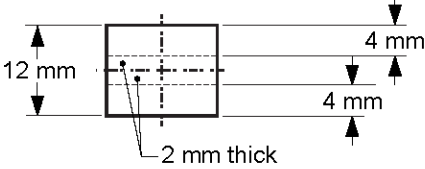
Figure 53.—Trend of thrust load to normal load ratio during testing interval #16 comprising 78,000 roller revolutions.

Figure 53 provides the trend of the axial force normalized to the normal force as a function of shaft revolutions for test interval #16 (the last testing interval). The operating speed during this test interval was 80 rev/min. The testing was completed over 2 working-day sessions comprising a total of 78,000 shaft revolutions. The lubrication was effective over the entire test interval. The trend of the axial force is similar to that of the first 80,000 cycles of interval #11 (Fig. 52). This test interval was stopped because the desired total number of durability cycles was completed.

Metallurgical Inspections

After the rollers completed the durability testing, the rollers were sectioned to inspect the material condition. The rollers sectioning actions are documented in Table 5. The pieces resulting from the sectioning are depicted in Figure 54. Also in Figure 54 are notations depicting the direction of view to inspect the section. Twelve sections were prepared and inspected. The photos to be presented will use the terms “circumferential” and “transverse” to denote sectioning orientation. The direction of rolling is in the plane of the view for a “circumferential section”. The rolling direction is perpendicular to the plane of view for a “transverse” section.

TABLE 5.—SECTIONING OF TESTED ROLLERS USING WIRE EDM

	Actions
1. Section each roller into 3 parts:	Step 1. Cut to create three annular sectors; preserved two sectors and used number three for further sectioning.
	Step 2. Cut sector number three into two sector pieces [became 3(A) and 3(B)].
2. Store sections 1 and 2 and cut section 3 into 2 parts:	Step 3. Cut piece 3(B) into four pieces, these cuts were perpendicular to the previous cuts.
	3(a). For case of the nitride 15-5 roller (N4), the cuts of piece 3(B) were equally spaced creating four pieces of nominally the same thickness.
3. Section part B into 4 parts:	3(b). For case of the 440C rollers (VRR100#7 and VRR100#8), the cuts of piece 3(B) were unequally spaced; cuts were made 4 mm from each end and the middle 4 mm piece cut in half again (2 mm thick each piece from middle section).
a. Roller "N4"	Note: The 440C roller VRR110#7 was used to propagate damage. The 440C roller VRR110#8 was used for the lubricated durability test.
	
b. Roller "VRR110#7" and "VRR100#8"	
	

Note: Each cut removed approximately 0.08 mm of material.

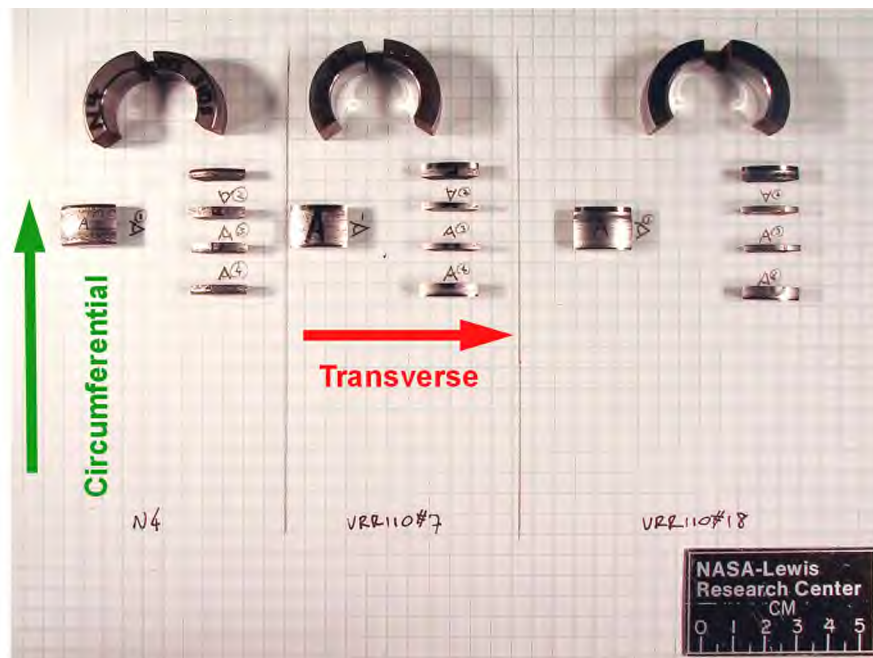


Figure 54.—Pieces created by sectioning of tested rollers for metallography inspections.

First will be discussed observations from cross sections of the nitrided 15-5 roller. Figure 55 provides transverse views (rolling direction perpendicular to the images). The figure shows two images, one from each of the two edges of the wear track. One can observe just outside the wear track (right side of Fig. 55(b)) the tightly adhered interface between the nitride layer and core material body. The nitride layer fractured in a brittle manner as expected from localized loads exceeding the material strength. In some regions the core 15-5 material was plastically displaced into the region of the nitride layer. In these views some penetrating cracks could be observed (an example shown in Fig. 55(a)). In all cases the penetrating cracks were shallow, blunted and turning transverse. Figure 56 provides circumferential views of three different sections on the nitride roller. The three views are from cuts made near each edge of the wear track (a) and (b) and near the middle of the wear track (c). In all of these three views, the brittle fracture of the nitride layer is evident. There are no penetrating cracks in these three views. In some cases, the fracture surface extended slightly into the core region and if this material became displaced would carry away a small amount of core material. In the center region (Fig. 56(c)), almost all of the nitride layer has been compromised and fractured and/or worn away.

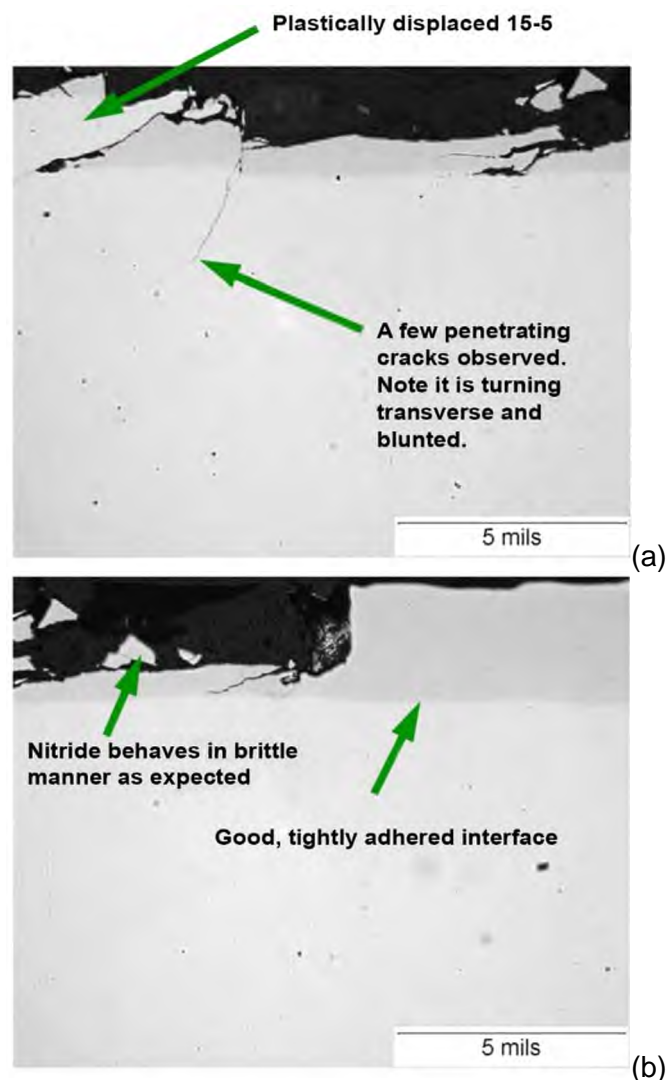


Figure 55.—Section views of the nitrided 15-5 roller near edges of wear track, transverse views (rolling perpendicular to the page). (a) Location 3 mm from edge closest to fastening nut. (b) Location 3 mm from edge closest to shaft shoulder.

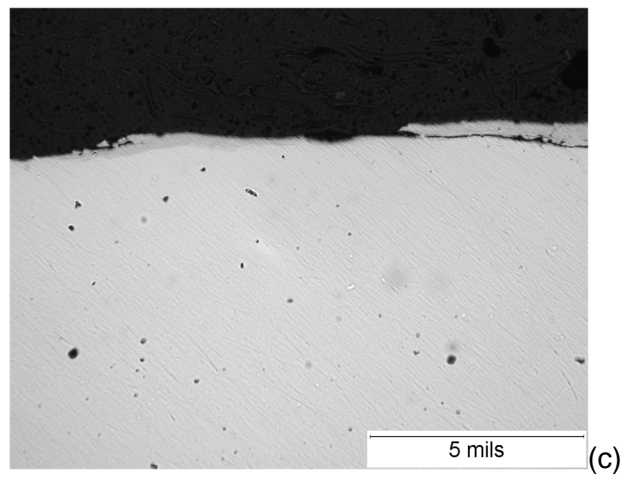
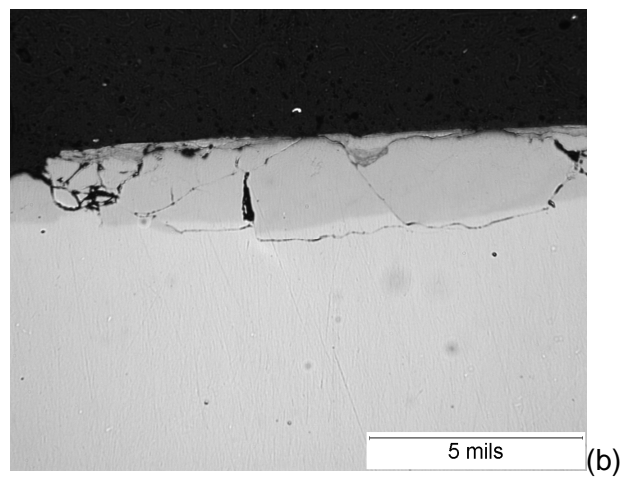
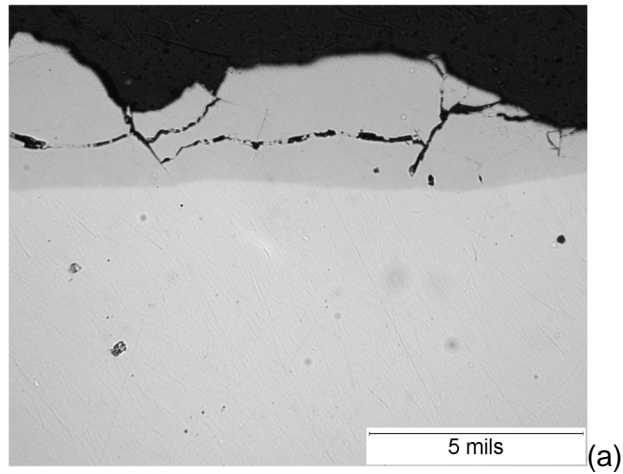


Figure 56.—Section views of the nitrided 15-5 roller, circumferential views (rolling direction within plane of page). (a) Location 3 mm from edge closest to fastening nut. (b) Location 3 mm from edge closest to shaft shoulder. (c) Location near middle of roller.

Figure 57 provides two section views of the 440C rollers, one section each of a transverse and circumferential view. Mild polishing wear is evident. The surface layer has predominantly ductile behavior. The wear is likely a mixture of abrasive polishing wear and adhesive wear. Any observed cracks were extremely shallow and within the debris layer. No penetrating cracks or other anomalies were observed. There were no indications or features found that could eventually compromise structural integrity of either the 440C or nitrided 15-5 roller.

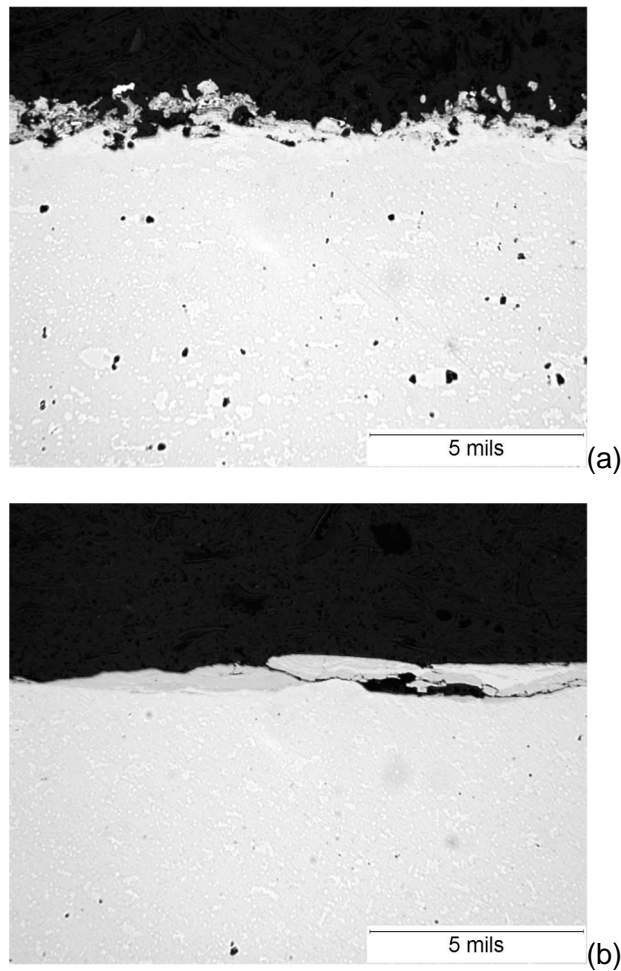


Figure 57.—Section views of the 440C roller. (a) Transverse view, rolling direction perpendicular to page. (b) Circumferential view.

Summary of Results

To provide some guidance on the expected behavior of the damaged SARJ ring with continued operations, experiments were conducted using rollers and a roller test rig. The approach of the experimental work involved three main steps: (1) initiate damage using conditions representative of the SARJ with inadequate lubrication; (2) propagate the damage by operating the test rollers without lubrication; and (3) assess the durability of the roller by testing to simulate the equivalent of 15 years of SARJ operation on the damaged surface assuming adequate grease lubrication. The durability test was completed comprising a total of 1.39 million shaft revolutions. The testing results were documented by occasional detailed inspections. Data collected and presented herein include visual assessment and documentation of the roller surface condition, tracking the mass of the rollers, stylus profilometer inspections, measurement and trending of the axial force at the contact, and metallographic sectioning and inspections at the end of the durability test. The following specific test results were obtained.

1. The damage initiation testing resulted in a compromise of the nitrided layer. The damage initiation test described herein demonstrates a plausible scenario for the damage of the SARJ ring. The damage depth was limited to the depth of the nitride layer.
2. The damage propagation testing demonstrated that the damage would propagate across the width of the roller. After the damage propagation testing the damage was considered as representative of the damaged SARJ ring.
3. From the visual assessments of the rollers and from the profilometer inspection, it was shown that the nitride layer would continue to fracture and wear away even after application of grease for lubrication.
4. The grease lubrication proved to be effective for limiting the value of the axial force that can be developed. Limiting the axial force on the SARJ mechanism is important since the larger the axial force the more concentrated the load pressure becomes on the blend-radius location on the SARJ roller.
5. With accumulation of cycles, the lubrication gradually became less effective as indicated by a rise in the axial force. Testing was paused at the end of a working day and restarted the next. These pauses in rotation correlated to a temporary reduction of the axial force. This temporary improvement of the lubrication condition perhaps was a result of reflow of oil into the contact region.
6. The depth of the damage for the nitrided roller after completion of the durability test was limited to about 0.2 mm. The depth of the nitride layer was about 0.15 mm. A relatively small amount of the core (un-nitrided) material was worn away.
7. The depth of the damage for the 440C roller after completion of the durability test was limited to about 0.06 mm, significantly less than the nitrided roller.
8. The structural integrity of the rollers was maintained. Metallographic inspections were done to search for indications of impending fatigue or other fracture indications that might eventually propagate and cause structural failure. There were no indications or features found that could eventually compromise structural integrity.

References

1. Loewenthal, S. and Schuller, F., "Feasibility study of a discrete bearing/roller drive rotary joint for the Space Station," NASA Technical Memorandum 8800, 1986.
2. Basta, Erin, et al., "Solar Alpha Rotary Joint Anomaly: The Materials and Processes Perspective," presentation to the Aging Aircraft Conference 2009.
http://ntrs.nasa.gov/archive/nasa/casi.ntrs.nasa.gov/20090017670_2009015384.pdf, accessed Nov. 17, 2009.
3. Olver, A.V., "The mechanism of rolling contact fatigue: an update," Proc. IMechE Vol. 219 Part J: J. Engineering Tribology, 2005.
4. Ingrassia, A. and Schwalbe, K.-H., Editors, "Special Issue on the Damage Tolerance of Railway Rails," Engineering Fracture Mechanics, Vol. 76, Issue 17, 2009.
5. Kalker, J.J., "Rolling contact phenomena: linear elasticity," Rolling Contact Phenomena CISM Courses and Lectures, Issue: 411, Springer-Verlag, 2000.
6. Wong, J.Y., Theory of Ground Vehicles, Wiley, New York, NY, 1978.
7. Vijayakar, S., "A Combined Surface Integral and Finite Element Solution for a Three-dimensional Contact Problem," International Journal for Numerical Methods in Engineering, 31, pp. 525-545, 1991.
8. McFatter, Justin, Private communication, 2009.
9. Moore, Lewis, Private communication, 2009.

